



OKLAHOMA TRANSPORTATION CENTER

*ECONOMIC ENHANCEMENT THROUGH INFRASTRUCTURE STEWARDSHIP*

# PROTOTYPE REINFORCED SOIL EMBANKMENT FOR RECONSTRUCTION OF US 62 SLOPE FAILURE IN CHICKASHA, OK

**KIANOOSH HATAMI, PH.D., P.E.**  
**GERALD A. MILLER, PH.D., P.E.**  
**DANIAL ESMALI**  
**EDMUND CHAN**

OTCREOS11.1-26-F

Oklahoma Transportation Center  
2601 Liberty Parkway, Suite 110  
Midwest City, Oklahoma 73110

Phone: 405.732.6580  
Fax: 405.732.6586  
[www.oktc.org](http://www.oktc.org)

**DISCLAIMER**

*The contents of this report reflect the views of the authors, who are responsible for the facts and accuracy of the information presented herein. This document is disseminated under the sponsorship of the Department of Transportation University Transportation Centers Program, in the interest of information exchange. The U.S. Government assumes no liability for the contents or use thereof.*

## TECHNICAL REPORT DOCUMENTATION PAGE

<b>1. REPORT NO.</b> OTCREOS11.1-26-F	<b>2. GOVERNMENT ACCESSION NO.</b>	<b>3. RECIPIENTS CATALOG NO.</b>	
<b>4. TITLE AND SUBTITLE:</b>  Prototype reinforced soil embankment for reconstruction of US 62 slope failure in Chickasha, OK		<b>5. REPORT DATE</b>  May 2013	
		<b>6. PERFORMING ORGANIZATION CODE</b>	
<b>7. AUTHOR(S) :</b> Kianoosh Hatami, Gerald A. Miller, Danial Esmaili, and Edmund Chan		<b>8. PERFORMING ORGANIZATION REPORT</b>	
<b>9. PERFORMING ORGANIZATION NAME AND ADDRESS</b>  School of Civil Engineering and Environmental Science, University of Oklahoma, Norman, OK 73019		<b>10. WORK UNIT NO.</b>	
		<b>11. CONTRACT OR GRANT NO.</b>  DTRT06-G-0016	
<b>12. SPONSORING AGENCY NAME AND ADDRESS</b>  Oklahoma Transportation Center (Fiscal) 201 ATRC Stillwater, OK 74078 (Technical) 2601 Liberty Parkway, Suite 110 Midwest City, OK 73110		<b>13. TYPE OF REPORT AND PERIOD COVERED</b>  Final Report, October 2011-May 2013	
		<b>14. SPONSORING AGENCY CODE</b>	
<b>15. SUPPLEMENTARY NOTES</b> University Transportation Center			
<b>16. ABSTRACT:</b> One of the main concerns in internal stability of reinforced soil structures constructed with fine-grained or marginal quality soils is the change in shear strength of the soil-reinforcement interface when the soil gravimetric water content (GWC) increases. This increase can occur during construction or service life of the structure, e.g. due to prolonged precipitation. The resulting loss in the soil matric suction could reduce the interface shear strength leading to serviceability problems or even failure of the reinforced soil structure. In this study, several 3.2 ft-high embankment models were constructed in the laboratory, which were subjected to strip footing loading in plane-strain condition. The embankment models were constructed using a lean clay at the GWC values ranging between OMC-2% and OMC+2% (OMC: Optimum Moisture Content). Each embankment model included a single reinforcement layer which was placed 7 inches below the embankment surface. The location of the reinforcement layer was selected based on preliminary embankment tests and numerical simulations to ensure that it would intercept the failure surface that developed underneath the strip footing near the embankment slope. The reinforcement was a woven geotextile material that had been used earlier by the authors in a series of pullout and interface shear tests on the same soil. The embankments were instrumented to measure the footing load, earth pressure, reinforcement strains and the soil GWC and matric suction values during the tests. A primary objective of the embankment tests was to investigate the influence of the soil as-compacted GWC value on the performance of the model embankments and thereby, validate or make necessary adjustments in the values of the moisture reduction factors (MRF) for reinforced embankment design that the authors had developed based on their prior pullout and interface shear tests.			
<b>17. KEY WORDS:</b> Soil slope structures, Unsaturated soils, Marginal soil, Geosynthetics, Moisture reduction factor		<b>18. DISTRIBUTION STATEMENT</b> No restrictions. This publication is available at <a href="http://www.oktc.org">www.oktc.org</a> and from NTIS.	
<b>19. SECURITY CLASSIF. (OF THIS REPORT)</b> Unclassified	<b>20. SECURITY CLASSIF. (OF THIS PAGE)</b> Unclassified	<b>21. NO. OF PAGES</b> . 73 + covers	<b>22. PRICE</b> N/A

## SI (METRIC) CONVERSION FACTORS

Approximate Conversions to SI Units				
Symbol	When you know	Multiply by	To Find	Symbol
<b>LENGTH</b>				
in	inches	25.40	millimeters	mm
ft	feet	0.3048	meters	m
yd	yards	0.9144	meters	m
mi	miles	1.609	kilometers	km
<b>AREA</b>				
in <sup>2</sup>	square inches	645.2	square millimeters	mm <sup>2</sup>
ft <sup>2</sup>	square feet	0.0929	square meters	m <sup>2</sup>
yd <sup>2</sup>	square yards	0.8361	square meters	m <sup>2</sup>
ac	acres	0.4047	hectares	ha
mi <sup>2</sup>	square miles	2.590	square kilometers	km <sup>2</sup>
<b>VOLUME</b>				
fl oz	fluid ounces	29.57	milliliters	mL
gal	gallons	3.785	liters	L
ft <sup>3</sup>	cubic feet	0.0283	cubic meters	m <sup>3</sup>
yd <sup>3</sup>	cubic yards	0.7645	cubic meters	m <sup>3</sup>
<b>MASS</b>				
oz	ounces	28.35	grams	g
lb	pounds	0.4536	kilograms	kg
T	short tons (2000 lb)	0.907	megagrams	Mg
<b>TEMPERATURE (exact)</b>				
°F	degrees Fahrenheit	(°F-32)/1.8	degrees Celsius	°C
<b>FORCE and PRESSURE or STRESS</b>				
lbf	poundforce	4.448	Newtons	N
lbf/in <sup>2</sup>	poundforce per square inch	6.895	kilopascals	kPa

Approximate Conversions from SI Units				
Symbol	When you know	Multiply by	To Find	Symbol
<b>LENGTH</b>				
mm	millimeters	0.0394	inches	in
m	meters	3.281	feet	ft
m	meters	1.094	yards	yd
km	kilometers	0.6214	miles	mi
<b>AREA</b>				
mm <sup>2</sup>	square millimeters	0.00155	square inches	in <sup>2</sup>
m <sup>2</sup>	square meters	10.764	square feet	ft <sup>2</sup>
m <sup>2</sup>	square meters	1.196	square yards	yd <sup>2</sup>
ha	hectares	2.471	acres	ac
km <sup>2</sup>	square kilometers	0.3861	square miles	mi <sup>2</sup>
<b>VOLUME</b>				
mL	milliliters	0.0338	fluid ounces	fl oz
L	liters	0.2642	gallons	gal
m <sup>3</sup>	cubic meters	35.315	cubic feet	ft <sup>3</sup>
m <sup>3</sup>	cubic meters	1.308	cubic yards	yd <sup>3</sup>
<b>MASS</b>				
g	grams	0.0353	ounces	oz
kg	kilograms	2.205	pounds	lb
Mg	megagrams	1.1023	short tons (2000 lb)	T
<b>TEMPERATURE (exact)</b>				
°C	degrees Celsius	9/5+32	degrees Fahrenheit	°F
<b>FORCE and PRESSURE or STRESS</b>				
N	Newtons	0.2248	poundforce	lbf
kPa	kilopascals	0.1450	poundforce per square inch	lbf/in <sup>2</sup>

# **PROTOTYPE REINFORCED SOIL EMBANKMENT FOR RECONSTRUCTION OF US ROUTE 62 SLOPE FAILURE IN CHICKASHA, OK**

**Final Report**

**May 2013**

**Kianoosh Hatami, Ph.D., P.E.**

**Associate Professor, Department of Civil Engineering & Environmental Science,  
The University of Oklahoma**

**Gerald A. Miller, Ph.D., P.E.**

**Professor, Department of Civil Engineering & Environmental Science,  
The University of Oklahoma**

**Danial Esmaili**

**Ph.D. Candidate, Department of Civil Engineering & Environmental Science,  
The University of Oklahoma**

**Edmund Chan**

**M.SC. Student, Department of Civil Engineering & Environmental Science,  
The University of Oklahoma**

**Sponsoring Agency**

**Oklahoma Transportation Center  
(Fiscal) 201 ATRC Stillwater, OK 74078  
(Technical) 2601 Liberty Parkway, Suite 110  
Midwest City, OK 73110**

# TABLE OF CONTENTS

EXECUTIVE SUMMARY .....	1
1. INTRODUCTION .....	2
2. OBJECTIVE AND SCOPE .....	4
3. EXTENDED MOHR-COULOMB FAILURE ENVELOPE.....	5
4. LITERATURE REVIEW.....	6
5. MATERIAL PROPERTIES AND INSTRUMENTATION.....	9
5.1 SOIL PROPERTIES .....	9
5.2 INSTRUMENTATION PLAN.....	14
5.2.1 PST-55 Psychrometer .....	14
5.2.2 EC-5 Sensors.....	14
5.2.3 WP4-T Water Potentiometer .....	15
5.2.4 Earth Pressure Cells (EPC) and Tactile .....	17
5.2.5 Thermocouples, Piezometers and Glass Beads .....	17
5.2.6 Wire Potentiometers and Linear Variable Differential Transformers (LVDT) .....	18
5.3 GEOSYNTHETIC REINFORCEMENT .....	21
6. REDUCED-SCALE EMBANKMENT TESTS .....	22
6.1 METHODOLOGY .....	22
6.1.1 Test Equipment.....	22
6.2 TEST PROCEDURE.....	25
6.2.1 Soil Processing .....	25
6.2.2 Construction of Model Embankments.....	28
6.2.3 Loading of Model Embankments and Dismantling of the Test Setup .....	31
6.2.4 Soil Gravimetric Water Content and Suction .....	33
6.2.5 Load-Settlement Data .....	43
6.2.6 Geotextile Strains.....	53
7. MOISTURE REDUCTION FACTOR, $\mu(\omega)$ .....	57
8. CONCLUSIONS.....	60
9. REFERENCES .....	61

## LIST OF FIGURES

Figure 1. US Route 62, Chickasha, OK; (a) Failed slope of a highway embankment, (b) Closer look at the location of the embankment failure.....	2
Figure 2. Soil sampling locations on U.S. Route 62, Chickasha, OK; (a) Cross section 2770, (b) Cross section 2780, and (c) Cross section 2790 and 2800.....	10
Figure 3. Gradation curves for the soil samples taken from CS 2780 at different depths as compared to that of the Chickasha soil (failed embankment soil). Note: the vertical broken line shows the location of #200 sieve.....	11
Figure 4. Compaction test results and SWCC for clay (ie. CS 2780) as compared to the Chickasha soil.....	13
Figure 5. WP4-T Water Potentiometer at the OU Geosynthetics Laboratory (soil samples in sealed cups are shown in the inset).....	15
Figure 6. Soil-Water Characteristic Curve for the test soil using WP4 Potentiometer as compared to the original soil from a failed embankment in Chickasha, OK. Note: red dashed lines show the OMC-2% and OMC+2% lines for the soil sample.....	16
Figure 7. Piezometer 1 placed in the 2 <sup>nd</sup> lift of the model embankment to measure possible changes in the soil pore water pressure.....	18
Figure 8. Instrumentation plan for reduced-scale reinforced embankment tests; (a) Cross sectional view, (b,c,d,e) Plan views. Note: <sup>(1)</sup> numbers in square brackets in (a) indicate the numbers of each sensors utilized for each test. <sup>(2)</sup> H, V, P and C in (a) stand for “horizontal”, “vertical”, “plan view” and “cross-sectional view”. <sup>(3)</sup> The distances between WP 1-WP 2 and WP 5-WP 6 are 2.5 inches and those between all other WPs are 3.5 inches.....	20
Figure 9. Mechanical response of the geotextile used in the pullout tests (Mirafi HP370) as per the ASTM D4595 test protocol and as compared with the manufacturer’s data (Hatami et al. 2010a). Note: The two arrows show the 5%-strain and ultimate tensile strength values of the geotextile reinforcement (1 kN/m = 68.5 lbs/ft).....	21
Figure 10. Test box and self-reacting loading frame fabricated for the reduced-scale reinforced embankment tests in this study.....	23

Figure 11. FLAC simulation of a reduced-scale reinforced embankment model; (a) Model at the end of construction, (b) Failure surface geometry in the embankment when subjected to strip footing load .....	25
Figure 12. Soil processing for reduced-scale embankment tests using a crusher-sifter machine .....	26
Figure 13. Soil mixing; (a) Mixing of soil to reach target gravimetric water content, (b) Sealed buckets containing processed soil before constructing the model embankment in the test box .....	27
Figure 14. Embankment construction; (a) Sealing of model embankment during construction to preserve its water content, (b) Trimmed front facing of the model embankment before applying the footing loading on the top .....	29
Figure 15. Locations of LVDTs for the reduced-scale embankment tests; (a) LVDTs to measure embankment deformation, (b) LVDTs to measure test box deformation .....	30
Figure 16. Placing the hydraulic cylinder at the center of footing and reaction beam in embankment tests .....	31
Figure 17. Failure surface after surcharge loading in the model embankment constructed at OMC-2% with woven geotextile HP370; (a) Before excavation, (b) After excavation of failure wedge .....	32
Figure 18. GWC data within the embankment from oven-drying method and PST-55 psychrometers; (a) Test case at OMC-2%, (b) Test case at OMC, and (c) Test case at OMC+2%. Notes: <sup>(1)</sup> Red dashed line shows the target GWC value, <sup>(2)</sup> Six (6) samples were taken from each layer to determine an average GWC value before compaction, <sup>(3)</sup> Three (3) random samples were taken immediately after compaction of 2-3 layers of embankment.....	35
Figure 19. Placement of the sensors before compaction of the layer .....	36
Figure 20. GWC data from EC-5 sensors in model embankments constructed at different GWC values; (a) Average GWC for each layer from EC-5 sensors at the end of construction (b) OMC-2%, (c) OMC and (d) OMC+2%. Note: The vertical red dashed line indicates the time when the loading started .....	40
Figure 21. GWC monitored using EC-5 sensors after construction and during loading; (a) OMC-2%, (b) OMC and (c) OMC+2% .....	43
Figure 22. Load- settlement data for test soil at different GWC values (OMC-2%, OMC, OMC+2%); (a) Individual settlement recorded by WP 7 and WP 8, (b) Average of settlement values from WP 7 and WP 8 .....	44

Figure 23. Displacements recorded during the embankment tests; (a) Lateral displacement of the test box near the top of the embankment (Figures 8a and 15b), (b) Vertical displacement of the embankment near the footing, (c) Horizontal displacement of the embankment's facing for the test case at OMC-2%, (d) Horizontal displacement of the embankment's facing for the test case at OMC .....	47
Figure 24. Comparison of the measured and theoretical predicted (Boussinesq method) incremental stresses due to the strip footing loading at selected locations in model embankments: (a) Test at OMC-2%, (b) Test at OMC .....	49
Figure 25. History of incremental earth pressures in the model embankment constructed at OMC subjected to footing loading.....	51
Figure 26. Changes in the pore water pressure as recorded by piezometers during surcharge loading: (a) Test at OMC-2%, (b) Test at OMC.....	52
Figure 27. Wire-line extensometers attached to geotextile reinforcement to measure geotextile strains.....	53
Figure 28. Geotextile displacements as measured with attached wire potentiometers for the test at OMC-2%; (a) Displacement recorded by WPs 1, 2 and 6, (b) Displacement recorded by WPs 3, 4 and 5 .....	54
Figure 29. Diagram of the reinforced embankment and the failure wedges observed in test cases at OMC-2%, OMC, and OMC+2%.....	55
Figure 30. Strain distributions in the geotextile reinforcement in different model embankments at failure load.....	56
Figure 31. (a) DST data on the embankment soil, (b) IST data on the embankment soil and woven geotextile.....	58
Figure 32. Moisture reduction factor, $\mu(\omega)$ , for the woven geotextile in the embankment models in this study (i.e. from the borrow source CS 2780 in Chickasha, OK) as compared to the corresponding IST values for the soil from a nearby failed roadway embankment in a recent study by the authors (Hatami et al. 2011b) .....	59

## LIST OF TABLES

Table 1. Properties of the soil sample taken from CS 2780 as compared to those of the original Chickasha soil .....	12
Table 2. Test information for reduced-scale reinforced embankments .....	22
Table 3. Material properties used in FLAC simulations.....	24

## EXECUTIVE SUMMARY

Oklahoma Department of Transportation (ODOT) and other departments of transportation in the U.S. are continually faced with a persistent problem of landslides and slope failures along highways. Repairs and maintenance work associated with these failures cost these agencies millions of dollars annually. Reinforced soil technology can provide viable solutions to stabilize or reconstruct highway slopes and embankments. However, a main concern in internal stability of reinforced marginal soils is the interface strength properties of reinforcement and soil when the soil gravimetric water content (GWC) increases significantly. This increase can occur during construction or due to prolonged precipitation. Wetting-induced reduction in matric suction and loss of shear strength in the soil and soil-reinforcement interface could lead to excessive deformation or complete failure of reinforced soil structures. In spite of such possibilities and actual failure occurrences, current design guidelines and test protocols for reinforced soil slopes (RSS) in North America do not include provisions to account for the reduction in interface shear strength due to increased gravimetric water content in the soil.

The proposed study is a natural extension of our recent and ongoing research funded by ODOT and OkTC which is aimed at developing design guidelines for reinforced soil slopes (RSS) constructed with locally available soils in unsaturated conditions and subjected to climatic factors in Oklahoma. In these studies, which have been reported in recent publications, moisture reduction factors (MRF) have been developed to account for the influence of the soil gravimetric water content and matric suction on the pullout resistance of a geotextile reinforcement material in two different marginal soils. One of these marginal soils is the soil from a failed highway embankment in Chickasha, OK, which is the subject of this report. The study described in this report involved construction and testing of three reduced-scale (3.2 ft high) prototype reinforced soil embankments at OU to study their performance and to validate the moisture reduction factors (MRF) for the soil-reinforcement interface response the authors obtained from the interface shear tests in their recent ODOT- and OkTC-supported studies in an actual embankment configuration. The validated MRF values can help make the equations involving soil-reinforcement interface shear strength for the design of mechanically stabilized earth (MSE) and reinforced soil slopes (RSS) with significant fines content more accurate and reliable.

# 1. INTRODUCTION

Landslides and slope failures along highways are a persistent problem across the U.S. Repairs and maintenance work associated with these failures cost national departments of transportation millions of dollars annually. In Oklahoma, many of these failures occur in the eastern and central parts of the state due to higher topography and poor soil types (Hatami et al. 2010a,b; 2011a,b). A recent example of these failures is a landslide on the US Route 62 (Figure 1) in Chickasha, Oklahoma. The landslide occurred due to precipitation and infiltration of rain water into the poorly-drained soil that caused increase in pore water pressure. Increase in pore water pressure will decrease the soil shear strength and slope stability.



(a)



(b)

Figure 1. US Route 62, Chickasha, OK; (a) Failed slope of a highway embankment, (b) Closer look at the location of the embankment failure

Design guidelines and specifications for Mechanically Stabilized Earth (MSE) structures in North America recommend the use of coarse-grained soils to repair and stabilize highway slopes and embankments (e.g., Elias et al. 2001; Berg et al. 2009). However, since coarse-grained soils are not commonly available in Oklahoma and many other parts of the U.S., depending on the location of the borrow source with respect to the project site, the costs of the fill material and its transportation can be prohibitive. In such cases, locally available soils could be considered as alternative construction materials because they would require less fuel consumption and generate less pollution compared to using high-quality offsite soils. It has been estimated that fuel costs constitute about 20% of the total costs for transportation of high-quality soil (Ou et al. 1982). Since commonly available soils for the construction of reinforced slopes in Oklahoma are of marginal quality (e.g., they contain more than 15% fines), they can be stabilized using geosynthetic reinforcement. The use of marginal soils in reinforced soil structures [e.g. mechanically stabilized walls (MSE) and reinforced soil slopes (RSS)] has been shown to reduce the cost of fill material by up to 60% (Keller, 1995). However, in order to reinforce earthen structures constructed with marginal soils, it is important to obtain satisfactory soil-reinforcement interface performance. The performance of marginal soils and their interface with geosynthetic reinforcement can be complex under construction or service loading conditions and may include excessive deformation and loss of strength as a result of wetting.

Important considerations in the design of reinforced soil structures constructed with marginal soils include reduction of interface shear strength and/or pullout resistance due to loss of soil suction (wetting), increases in gravimetric water content and possible development of excess pore water pressure. These factors can result in excessive deformations and even failure of reinforced soil structures. Therefore, design procedures for reinforced soil structures need to take into account the influence of soil suction on the soil strength, the strength of the soil-geosynthetic interface and the resulting factor of safety against failure. Such design provisions are currently not available for reinforced soil structures constructed with marginal soils.

Typically, construction materials for reinforced soil structures are tested at gravimetric water content values near optimum (i.e., Optimum Moisture Content - OMC). However, in actual construction, several factors could cause the fill gravimetric water content to deviate from the design value. Examples include precipitation during construction, groundwater infiltration and development of excess pore water pressure due to compaction. These factors, in addition to seasonal variations of soil water content, can significantly reduce the strength of the soil-reinforcement interface and lead to excessive deformations or failure.

## 2. OBJECTIVE AND SCOPE

The pullout capacity of reinforcement and interface shear strength in a soil mass are the important factors in stability analysis and design of reinforced soil structures. For internal stability, pullout resistance of the reinforcement,  $P_r$ , and interface shear strength of soil and reinforcement are determined using Equations 1 and 2, respectively:

$$P_r = F^* \alpha \sigma'_v L_e C \quad (1)$$

$$\tau = c_a + \sigma'_v \tan \delta \quad (2)$$

Where  $F^*$ ,  $\alpha$ ,  $\sigma'_v$ ,  $L_e$ ,  $C$ ,  $\tau$ ,  $c_a$  and  $\delta$  are pullout resistance factor, stress distribution correction factor, effective vertical stress at soil-reinforcement interface, reinforcement anchorage length, effective unit perimeter (e.g.  $C=2$  for strips, grids and sheets), interface shear strength, interface adhesion and interface friction angle, respectively. The hypothesis of this study is that changes in matric suction and gravimetric water content due to wetting of the soil-reinforcement interface could significantly influence the pullout capacity of the fabric and/or interface shear strength of the soil and fabric as determined from Equations 1 and 2. Therefore, a moisture factor,  $\mu(\omega)$ , needs to be applied in Equations 1 and/or 2 to account for the variation of gravimetric water content and suction on the unsaturated soil-reinforcement interface strength (Equations 3 and 4):

$$P_r = F^* \alpha \sigma'_v L_e C \mu(\omega) \quad (3)$$

$$\tau = [c_a + \sigma'_v \tan \delta] \mu(\omega) \quad (4)$$

In a recent study by the authors and colleagues (Hatami et al. 2010a,b; 2011a,b), a moisture reduction factor [MRF or  $\mu(\omega)$ ] was developed for two different Oklahoma soils (i.e. Minco silt and Chickasha clay) using pullout and interface shear tests (IST) in the laboratory. The present study was aimed at validating the equations for  $\mu(\omega)$  from IST using the performance of model reinforced embankments under surcharge loading in the laboratory. The study involved construction and testing of three reduced-scale (3.2 ft high) reinforced soil embankment models at OU to study their performance and to validate, in embankment configuration, the  $\mu(\omega)$  factors that were obtained previously from the interface shear and pullout tests in the laboratory.

### 3. EXTENDED MOHR-COULOMB FAILURE ENVELOPE

The shear strength of an unsaturated soil depends on two stress variables: net normal stress ( $\sigma_n - u_a$ ) and soil matric suction ( $u_a - u_w$ ) (Fredlund et al. 1978). The net normal stress is the difference between the total stress and pore air pressure, and the matric suction is the difference between the pore air and the pore water pressures. Miller and Hamid (2005) proposed the following equation to determine the shear strength of unsaturated soil-structure interfaces:

$$\tau_s = C'_a + (\sigma_n - u_a) \tan \delta' + (u_a - u_w) \tan \delta^b \quad (5)$$

Where:

- i.  $C'_a$ : Adhesion intercept
- ii.  $\sigma_n$ : Normal stress on the interface
- iii.  $u_a$ : Pore air pressure
- iv.  $\delta'$ : The angle of friction between soil and reinforcement with respect to  $(\sigma_n - u_a)$
- v.  $u_w$ : Pore water pressure
- vi.  $\delta^b$ : The angle of friction between soil and reinforcement with respect to suction  $u_a - u_w$

In the case of an unsaturated soil, Mohr's circles representing failure conditions correspond to a 3D failure envelope, where the shear stress ( $\tau$ ) is the ordinate and the two stress variables are the abscissas  $(\sigma_n - u_a)$  and  $(u_a - u_w)$ . The locations of the Mohr's circles in the third dimension are functions of matric suction  $(u_a - u_w)$ . The planar surface formed by these two stress variables is called the extended Mohr-Coulomb failure envelope.

## 4. LITERATURE REVIEW

A survey of related literature that was carried out during the course of this study is summarized in this section.

Huang et al. (1994) tested a series of reinforced and unreinforced sand slopes subjected to footing loading. Their results showed that the bearing capacity of the footing increased when reinforcement layers were placed within the active wedge. They also found that the bearing capacities and failure patterns of the reinforced slopes were dependent on the arrangement of reinforcement members.

Adams et al. (1997) conducted large-scale model footing load tests on a frictional soil reinforced with geogrids and geocells. In their study, they varied factors such as the number of reinforcement, reinforcement spacing, soil density, reinforcement type and the depth of the first reinforcement layer. Their results showed that geosynthetic reinforcement could increase the ultimate bearing capacity of shallow spread footings by a factor of 2.5.

Lee et al. (1999) studied the influence of geotextile reinforcement and the thickness of sand layer on ultimate bearing capacity and settlement behavior of a footing supported on soft clay overlain by granular fill (sand). Their results showed that the foundation bearing capacity increased with the ratio of sand layer thickness to footing width up to 0.8 (which was called the optimum thickness of the sand layer). Their study also showed that the use of a geotextile reinforcement layer at the interface between the sand and clay significantly improved the footing bearing capacity and decreased its settlement.

Lee and Manjunath (2000) examined the influence of geosynthetic reinforcement on the bearing capacity of footings on sloped embankments. Their study confirmed that the load-settlement behavior and ultimate bearing capacity of the footing could be improved significantly as the reinforcement layer was installed at an optimum depth within the slope. Their test data indicated that the optimum depth of reinforcement layer was 0.5 times the width of the footing ( $B$ ). The study also showed that when the distance between the footing and the slope crest was less than five times the width of the footing ( $5B$ ), the footing bearing capacity decreased as the slope angle increased and the footing distance from the slope edge decreased. Beyond  $5B$ , the bearing capacity of the footing was found to be practically independent of the distance between the footing and the slope.

Bathurst et al. (2003) studied the performance of reinforced and unreinforced slopes under a strip footing load. Their study showed that an increase in the reinforcement length and stiffness increased the ultimate load capacity of the strip footing. Their results also indicated that the bearing capacity of the reinforced embankment was up to two times as large as that of an otherwise identical unreinforced embankment.

Kumar and Saran (2003) carried out several tests on closely spaced strip and square footings resting on geogrid-reinforced sand to study the influence of footing spacing and reinforcement size and continuity of reinforcement on the bearing capacity and rotation of the footing. Their results showed a significant improvement in bearing capacity and settlement of strip footings when continuous reinforcement layers were used in the models. However, the improvement in the case of square footings was found to be rather insignificant. Their data showed that both strip and square footings experienced less tilting when continuous reinforcement was placed in the soil.

Sitharam et al. (2005) performed a series of laboratory loading tests on a circular footing placed on a geocell-reinforced clay to investigate the influence of the geocell layer depth and the width and height of the geocell on the foundation bearing capacity. Their test results showed that using geocell reinforcement layer could improve the bearing capacity of soft clay by a factor of 4.8 as compared to unreinforced clay. Their results also indicated that a sufficiently deep and wide geocell could also decrease the swelling of the soft clay significantly.

Sako et al. (2006) performed numerical analyses to investigate the failure mechanism of unsaturated soil slopes due to increases in saturation. Their results showed that the slope failure was preceded by a rapid increase in the pore water pressure. It was also observed that as the soil became more saturated, the factor of safety against slope failure decreased.

Kumar et al. (2007) performed a series of tests on a strip footing rested on a reinforced layered sand to determine its ultimate bearing capacity. The foundation consisted of a strong sand layer overlying a low bearing capacity sand deposit. They observed that replacing the top 1B-thick layer of the weak soil (B is the strip footing width) with well-graded sand reinforced with 2 to 4 layers of geogrid reinforcement could increase the ultimate bearing capacity of footing up to 4 times and reduce the footing settlement.

Tohari et al. (2007) carried out a series of tests on laboratory-scale soil slopes to investigate the effects of rainfall on slope failure. The dominant failure mode was found to be a shallow noncircular slip surface after formation of a seepage zone near the slope toe. Tohari et al. found that although the zones of localized failure reached a saturated state, the major part of the unstable soil slope remained unsaturated.

Germer et al. (2008) investigated the effect of saturation on the development of failure processes within a soil slope. Their results showed that the slope could sustain 20% more load to reach failure when the shear band had negative pore pressure as compared to the case where the shear band was below the ground water level.

Thanapalasingam and Gnanendran (2008) performed a numerical analysis to study the effects of using multiple layers of reinforcement and to determine the most effective layout for reinforced slopes. Their study indicated that the locations and spacing of the reinforcement layers are key factors to improve the load-displacement response of footing on a slope. Thanapalasingam and Gnanendran's results showed that the ultimate bearing capacity of footing improved significantly by increasing the number of reinforcement layers. The maximum footing load was observed when the spacing between the two reinforcement layers in the 3 ft-high model embankments was equal to the footing width.

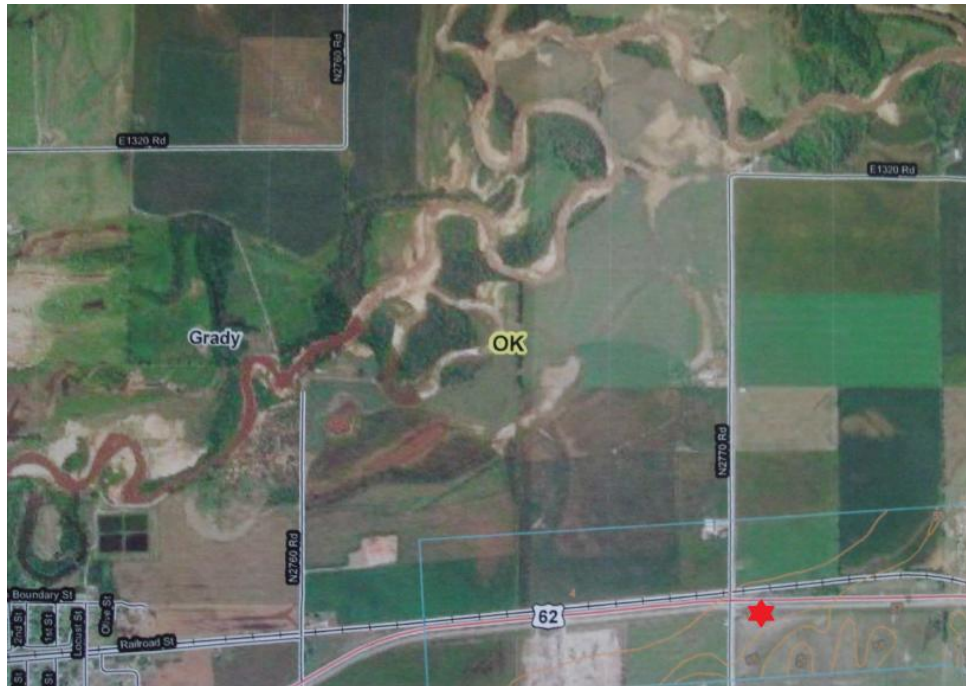
Georgiadis (2010) studied the undrained bearing capacity of a strip footing on a slope as a function of the footing width, its distance from the slope and the slope height using the finite element method. Their results indicated that three different failure modes could occur depending on the height of slope ( $H$ ) relative to the footing width ( $B$ ). The results showed that at low  $H/B$  ratios, the failure surface was restricted by the slope height and when the  $H/B$  values placed between 0.25 and 0.75, failure surface extended to the slope and was not affected by  $H$  values. The third failure mode involved overall slope failure at high values of  $H/B$ . The study also indicated that the undrained bearing capacity of the footing increased with its distance from slope.

Sawwaf and Nazir (2012) studied the behavior of an eccentrically loaded ring footing on a geogrid-reinforced compacted sand which overlaid loose sand. Their test results showed that the behavior of the ring footing improved considerably as the thickness and relative density of compacted sand layer increased. Their investigation also confirmed that using geosynthetic reinforcement could reduce the required thickness of compacted sand and/or lead to increased bearing capacity of the footing.

## 5. MATERIAL PROPERTIES AND INSTRUMENTATION

### 5.1 SOIL PROPERTIES

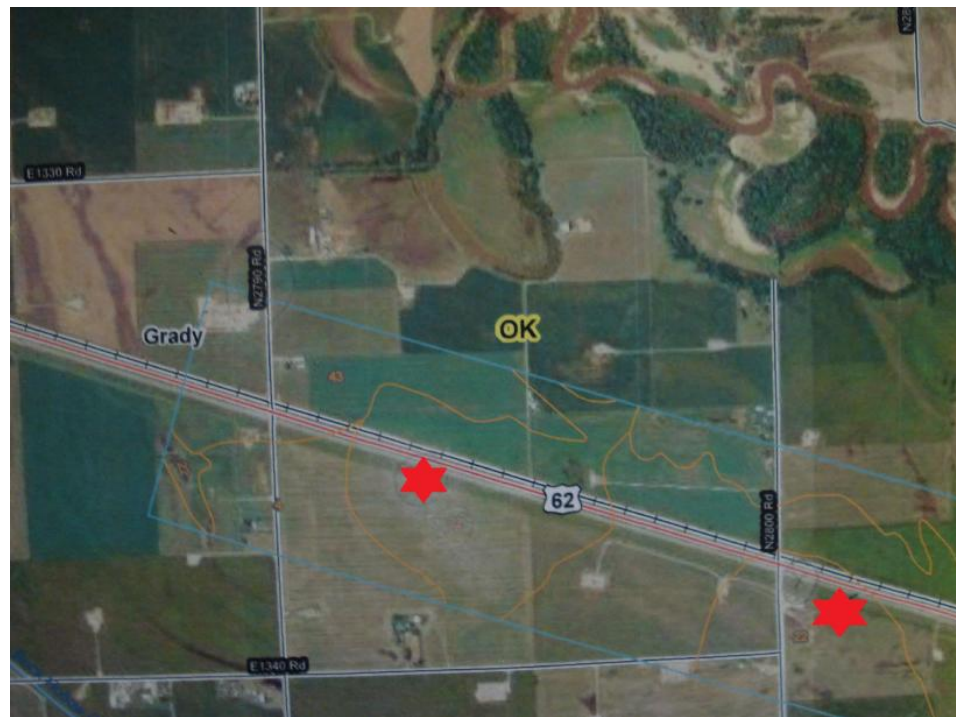
A significant amount of soil from the Chickasha highway slope failure site (on the order of 5 cubic yards) was required for the reduced-scale embankment tests. Obviously, it was not feasible to collect such amount of soil at the Chickasha highway embankment site. Therefore, the Web Soil Survey (WSS) online utility was used and four alternative sources of soil near the Chickasha site were identified that indicated properties similar to those of the embankment soil. A trip was made to the area near the Chickasha highway embankment site by the research group and met up with Dr. Jim Nevels to inspect the sites closely and take some soil samples. The soil that was used originally in the construction of the embankment is categorized as McLain Series which is primarily a thick layer of silty clay material (weathered loamy alluvium). The locations where the soil samples were taken are marked with red stars in Figure 2. These areas are located on U.S. Route 62 at cross section numbers 2770, 2780, 2790 and 2800. The soil samples were taken from depths between 7 inches and 50 inches below the ground surface and were transported to the soils laboratory at OU for testing and classification.



(a)



(b)



(c)

Figure 2. Soil sampling locations on U.S. Route 62, Chickasha, OK; (a) Cross section 2770, (b) Cross section 2780, and (c) Cross section 2790 and 2800

Physical and mechanical soil property tests were carried out on the soil samples taken from the four candidate cross sections identified near the borrow source locations in Chickasha (i.e. CS 2770, 2780, 2790 and 2800) in general accordance with ASTM D1140 and ASTM D422 to determine the soil gradation and fines content. The laboratory test results showed that the liquid limit (LL), plastic limit (PL) and the plasticity index (PI) values of the soil located at CS 2780 (i.e. 39, 22 and 17, respectively) were comparable with those of the Chickasha soil at the roadway embankment site (i.e. LL=38, PL=20 and PI=18). Figure 3 shows the gradation curves from sieve analysis and hydrometer tests for the soil samples taken from different depths at the CS 2780 location. The soil from this borrow source is classified as CL and A-6 according to the Unified Soil Classification System (USCS) and AASHTO, respectively, which is the same as the soil from the failure site. Table 1 shows a comparison of the soil properties for the sample from CS 2780 as compared to those of the Chickasha soil at the failed embankment site.

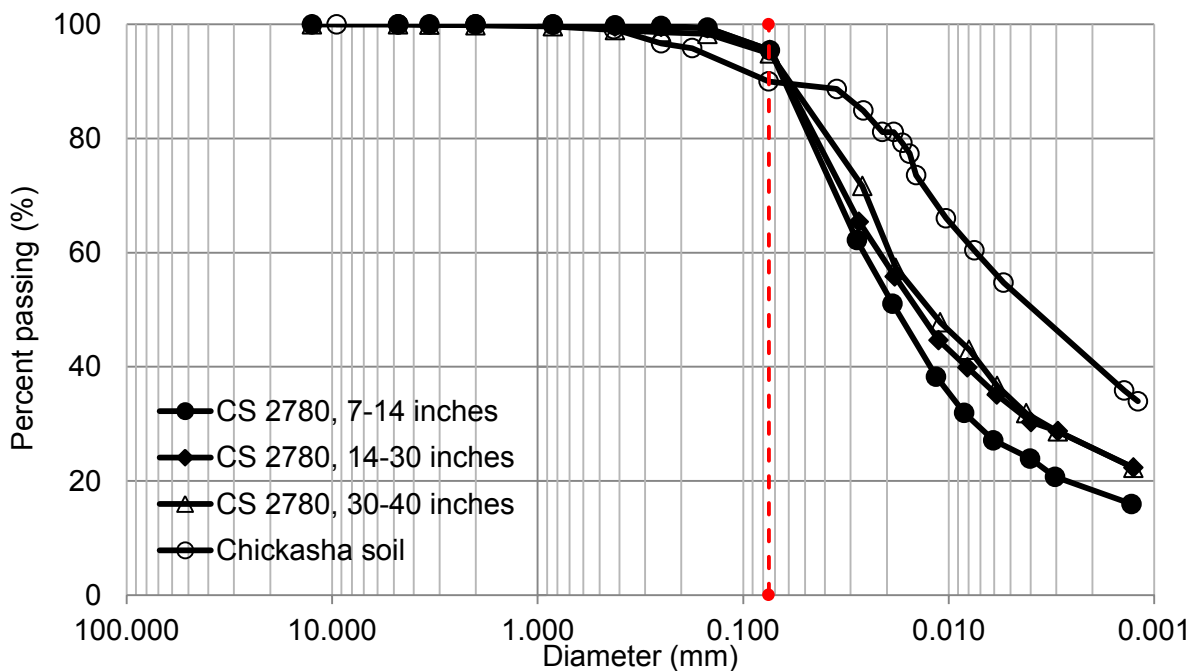


Figure 3. Gradation curves for the soil samples taken from CS 2780 at different depths as compared to that of the Chickasha soil (failed embankment soil). Note: the vertical broken line shows the location of #200 sieve

Table 1. Properties of the soil sample taken from CS 2780 as compared to those of the original Chickasha soil

Property	Chickasha soil	CS 2780
<b>Liquid Limit (%)</b>	38	39
<b>Plastic Limit (%)</b>	20	22
<b>Plasticity Index (%)</b>	18	17
<b>Specific Gravity</b>	2.75	2.75
<b>Sand (%)</b>	10.6	4.8
<b>Silt (%)</b>	49.4	69.2
<b>Clay (%)</b>	40	26
<b>Maximum Dry Unit Weight, pcf (kN/m<sup>3</sup>)</b>	111 (17.3)	120 (18.8)
<b>Optimum Moisture Content (%)</b>	18	15

A modified proctor test was carried out on the CS 2780 soil to determine the values of its maximum dry unit weight and optimum moisture content (

Figure 4. Compaction test results and SWCC for clay (ie. CS 2780) as compared to the Chickasha soil  
 ).

Figure 4. Compaction test results and SWCC for clay (ie. CS 2780) as compared to the Chickasha soil

also shows a series of theoretical curves of the soil dry unit weight versus gravimetric water content (GWC) for different degrees of saturation. The values of maximum dry unit weight for these curves were obtained from Equation 6:

$$\gamma_d = \frac{G_s}{1 + \frac{\omega G_s}{S}} \gamma_w \quad (6)$$

Where:

- i.  $G_s$ : Specific gravity
- ii.  $\omega$ : GWC
- iii.  $S$ : Degree of saturation
- iv.  $\gamma_w$ : Water unit weight

- v.  $\gamma_d$ : Soil dry unit weight

The curves corresponding to  $S = 1, 0.9$  and  $0.8$  are shown as the zero air void line (ZAVL - representing the minimum void ratio attainable at a given GWC value), 10% AVL and 20% AVL, respectively (Budhu 2000). The air void lines in Figure 4. Compaction test results and SWCC for clay (ie. CS 2780) as compared to the Chickasha soil

were determined using Equation 6. To plot the ZAVL, the soil saturation was set to unity ( $S = 1$ ). Then, having specific gravity for the soil from Table 1 ( $G_s = 2.75$ ) and water unit weight ( $\gamma_w = 10 \text{ kN/m}^3$ ), the dry unit weight ( $\gamma_d$ ) was calculated at different gravimetric water content ( $\omega$ ) values. This procedure was repeated to obtain the 5%, 10%, 15% and 20% air void lines.

Figure 4. Compaction test results and SWCC for clay (ie. CS 2780) as compared to the Chickasha soil

shows that the maximum dry unit weight was attained at  $S = 0.9$  and also, the test results are reliable because the wetting points are placed below the ZAVL.

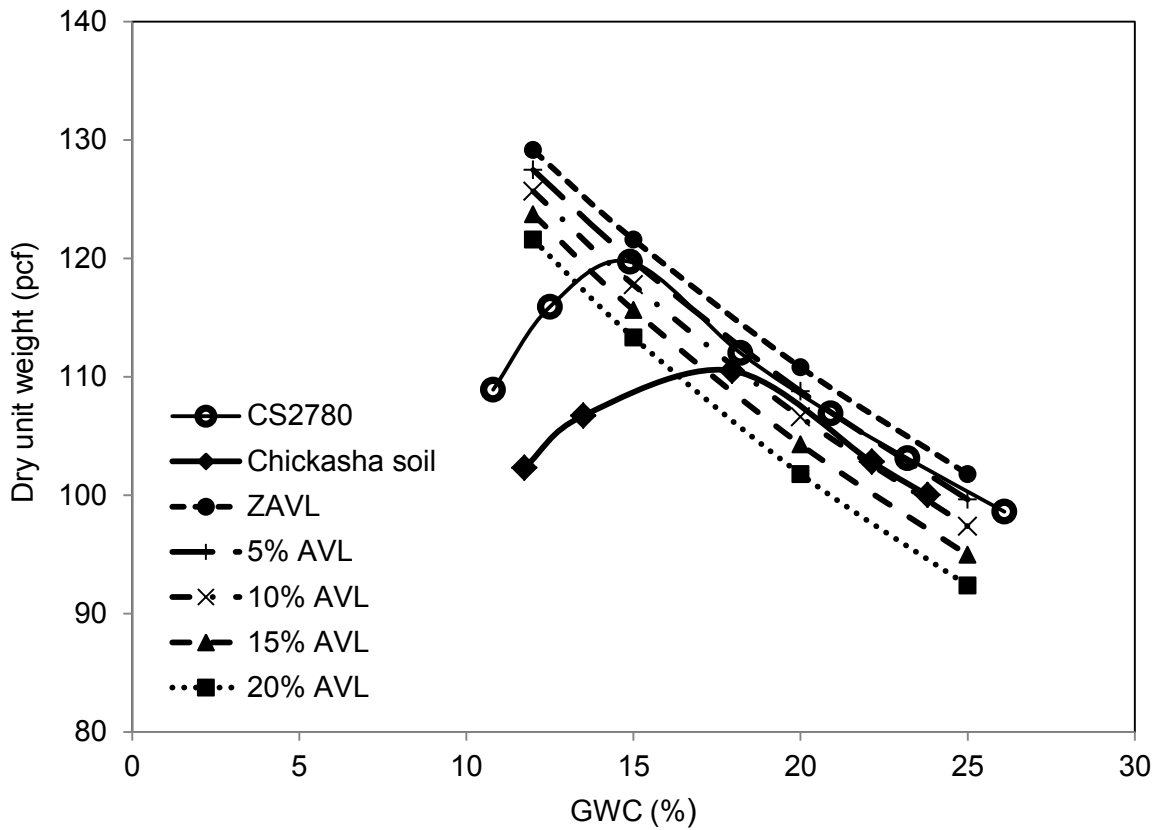


Figure 4. Compaction test results and SWCC for clay (ie. CS 2780) as compared to the Chickasha soil

## 5.2 INSTRUMENTATION PLAN

In this study, different sensors were used to measure the soil suction, gravimetric water content, earth pressure, temperature, embankment deformation and geotextile strain as described in the following sections:

### 5.2.1 PST-55 Psychrometer

PST-55 is an in-situ psychrometer which can measure total suction in the soil up to 5000 kPa. Under vapor equilibrium conditions, water potential in the porous cup of the instrument is directly related to the vapor pressure of the surrounding air. This means that the soil water potential is determined by measuring the relative humidity of the chamber inside the porous cup (Campbell et al. 1971). PST-55 psychrometer sensors can lose their factory calibration over time. Therefore, in this study we calibrated them using a 1000 mmol/kg NaCl solution before we used them in the pullout tests. The sensors were submerged in NaCl solutions and kept in an ice chest for about 2 hours to reach equilibrium (Wescor Inc. 2001). The ice chest provided a controlled temperature and moisture environment for the calibration of the sensors. Afterwards, each sensor was connected to a dew point microvoltmeter model HR-33T (one at a time) and the water potential of the control NaCl solution was read in microvolts( $\mu V$ ).

### 5.2.2 EC-5 Sensors

The capabilities of several different sensors were examined to measure the gravimetric water content (GWC) in the embankment soil based on the past experience in pullout and interface shear tests and the available literature. Example sensors surveyed in the literature included models 5-TE, EC-5, 10-HS, 5-TM, Hydra probe, SM-300 and Theta probe. Major factors that were the focus of this study included the sensor size, measuring range, precision and cost. The objective was to look for the smallest sensor that would operate over a wide range of GWC values and would be suitable for different types of soils. Based on the specifications and capabilities reported in the literature and prior experience, the EC-5 sensors were chosen to measure the GWC in the embankment models. The EC-5 sensors were installed in the vicinity of the soil-reinforcement interface to monitor changes in the soil GWC value in that part of the embankment models before, during and after each test. EC-5 sensors are capable of continuous reading of the soil volumetric water content which is related to the GWC through the following relationship (Equation 7):

$$\theta_v = \omega \times \frac{\rho_d}{\rho_w} \quad (7)$$

Where:

- i.  $\theta_v$ : Volumetric water content

- ii.  $\omega$ : GWC
- iii.  $\rho_d$ : Dry density of the soil
- iv.  $\rho_w$ : Density of water

### 5.2.3 WP4-T Water Potentiometer

The WP4 Potentiometer measures the soil total suction. It consists of a sealed block chamber equipped with a sample cup, a mirror, a dew point sensor, a temperature sensor, an infrared thermometer and a fan (Figure 5). The soil sample is placed in the sample cup and brought to vapor equilibrium with the air in the headspace of the sealed block chamber. At equilibrium, the water potential of the air in the chamber is the same as the water potential or suction of the soil sample.

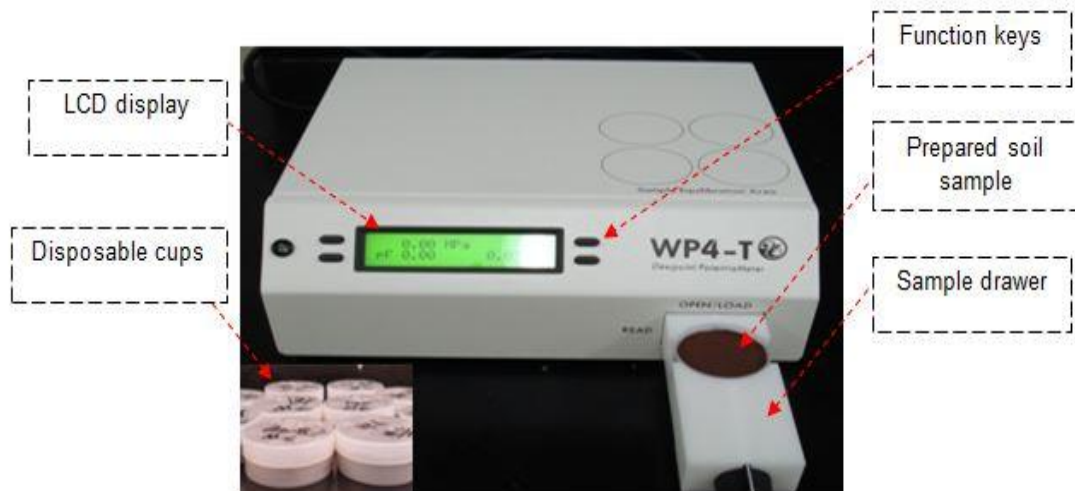


Figure 5. WP4-T Water Potentiometer at the OU Geosynthetics Laboratory (soil samples in sealed cups are shown in the inset)

Fifteen (15) samples of the embankment soil were prepared at different GWC values. The soil was used to make a 1.57 inch (diameter) by 0.24 inch (height) sample for the WP4 potentiometer at the same dry unit weight as was used in the embankment tests. The WP4 samples were placed in sealed disposable cups (Figure 5). Before testing each soil sample using WP4, a salt solution of known water potential (0.5 molal KCl in H<sub>2</sub>O) was used to calibrate the WP4 sensor. For each test, the sample was placed inside the WP4 sample drawer and was allowed to reach temperature equilibrium with the equipment internal chamber. Then, the knob

on the tray was turned to the “READ” position to read the water potential of the soil sample. The magnitude of the soil total suction was recorded once the displayed reading stabilized at a constant value. **Error! Reference source not found.** shows the Soil-Water Characteristic Curve (SWCC) for the test soil (from the CS2780 borrow source) that was obtained through WP4 tests as compared to the original (i.e. failed embankment) Chickasha soil.

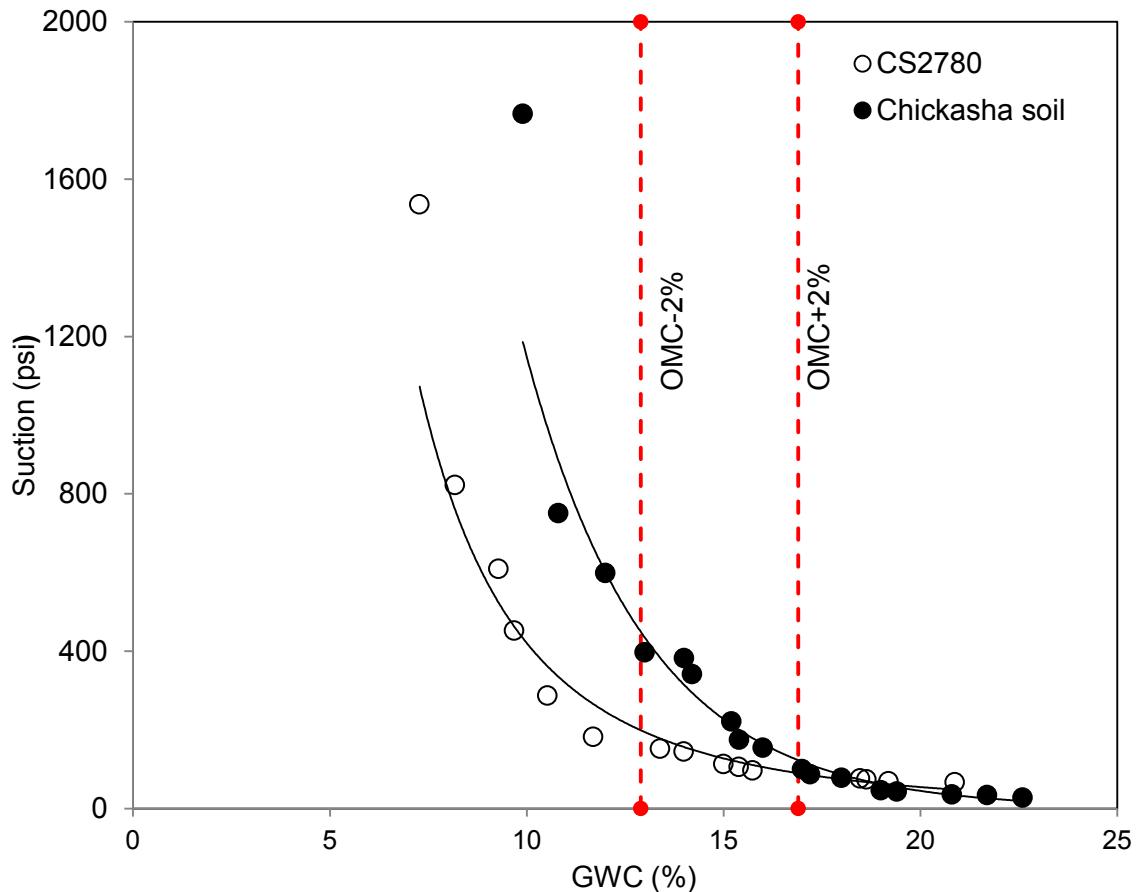


Figure 6. Soil-Water Characteristic Curve for the test soil using WP4 Potentiometer as compared to the original soil from a failed embankment in Chickasha, OK. Note: red dashed lines show the OMC-2% and OMC+2% lines for the soil sample

#### 5.2.4 Earth Pressure Cells (EPC) and Tactile

Two earth pressure cells (EPC) (i.e. Geokon model 4800) were used to measure the vertical and lateral earth pressures inside the embankment. Another Geokon “fatback” EPC (Model 4810) was used to measure the vertical earth pressure at the bottom of the test embankment. In addition to the EPC, twenty four (24) 1.7-in.-diameter free-form tactile pressure sensors (TPS, Sensor Prod 2013) were used to measure earth pressure at various locations in the embankment. The flexibility and small surface area of the tactile pressure sensors were

advantageous in that these attributes helped minimize the influence of their physical presence on the initiation and growth of the failure surface in the embankment models during the embankment models surcharge loading tests.

### **5.2.5 Thermocouples, Piezometers and Glass Beads**

The temperature at different locations within the embankment was monitored using three (3) thermocouples to determine the accuracy of readings from different sensors because the calibration factors for most sensors used in the embankment tests were valid for predetermined temperatures.

Two piezometers were installed within the embankment to monitor any possible excess pore water pressure due to loading. Due to their comparatively large size, the piezometers were placed horizontally (Myers and Scofield 2006.) at sufficient distances from the loading beam inside the embankments so that they would not interfere with the stress distribution and embankment deformation during the surcharge loading stage of the test (Figure 7). Nineteen (19) 0.4-in.-diameter glass beads were placed inside the embankment models to monitor the internal movements of the embankment soil (Figure 8).

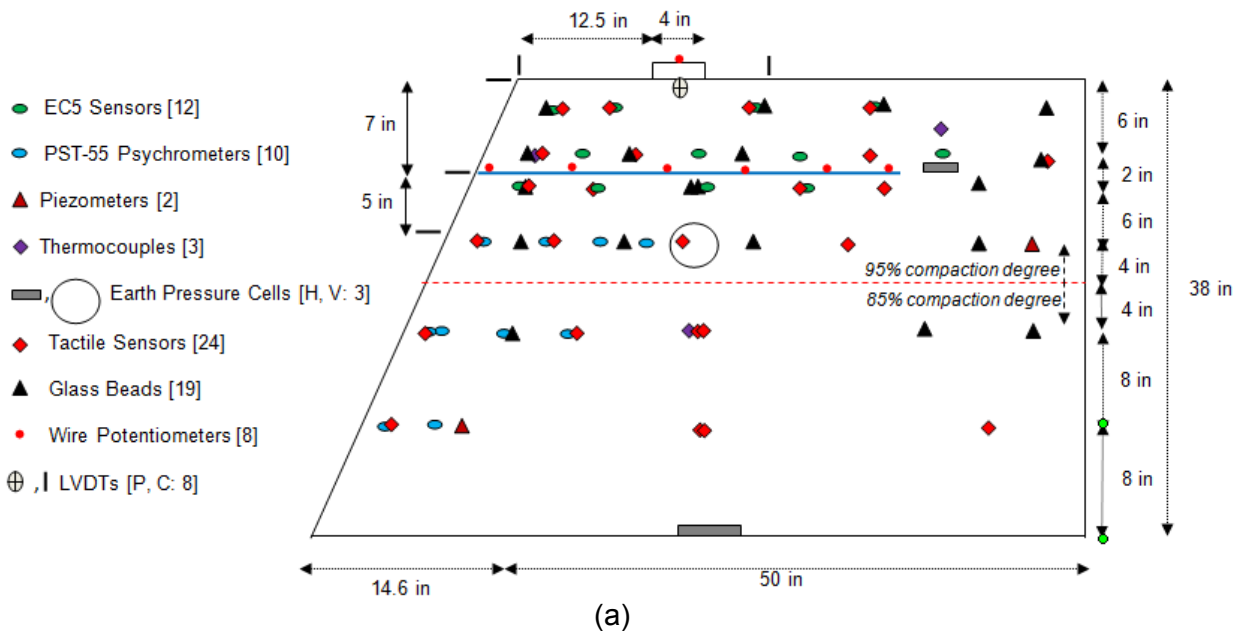


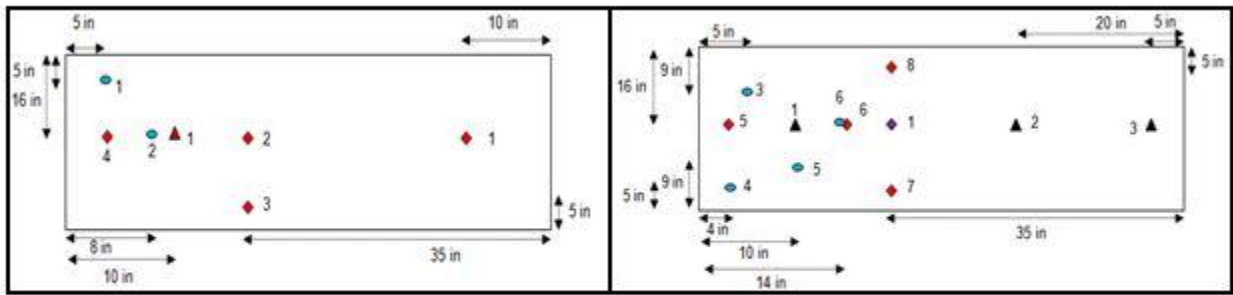
Figure 7. Piezometer 1 placed in the 2<sup>nd</sup> lift of the model embankment to measure possible changes in the soil pore water pressure

### 5.2.6 Wire Potentiometers and Linear Variable Differential Transformers (LVDT)

Six (6) Celesco PT101 cable extension position transducers (wire potentiometers) were used to determine the geotextile strains. The PT101 transducer has a precision potentiometric output with a range of 0 to 10 inches and an accuracy of up to 0.1% of full scale. Two more wire potentiometers were installed on the strip footing to monitor the footing settlement while loading the embankment until failure.

The deformation of the embankment along its facing and top surface was monitored and measured using six (6) LVDTs. Two (2) additional LVDTs were used to measure the lateral deformation of the test box to check the symmetric behavior of the test setup. Figure 8 shows the schematic diagram of the instrumentation plan for the embankment tests.

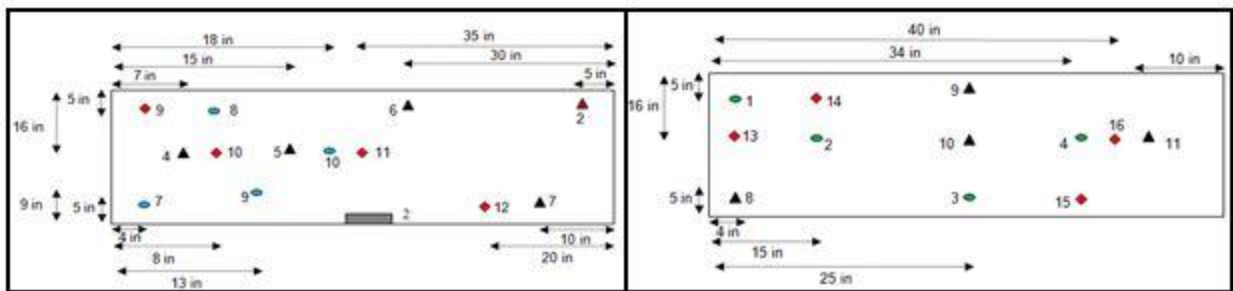




H= 8 in

H= 16 in

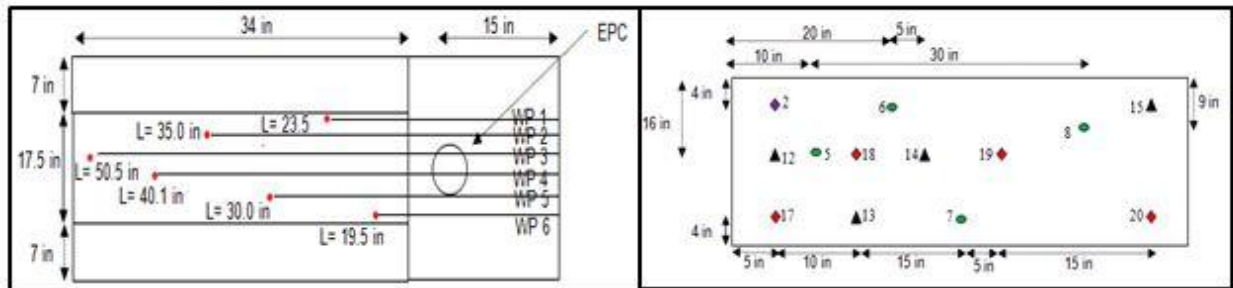
(b)



H= 24in

H= 30 in

(c)



H= 31 in

H= 32 in

(d)



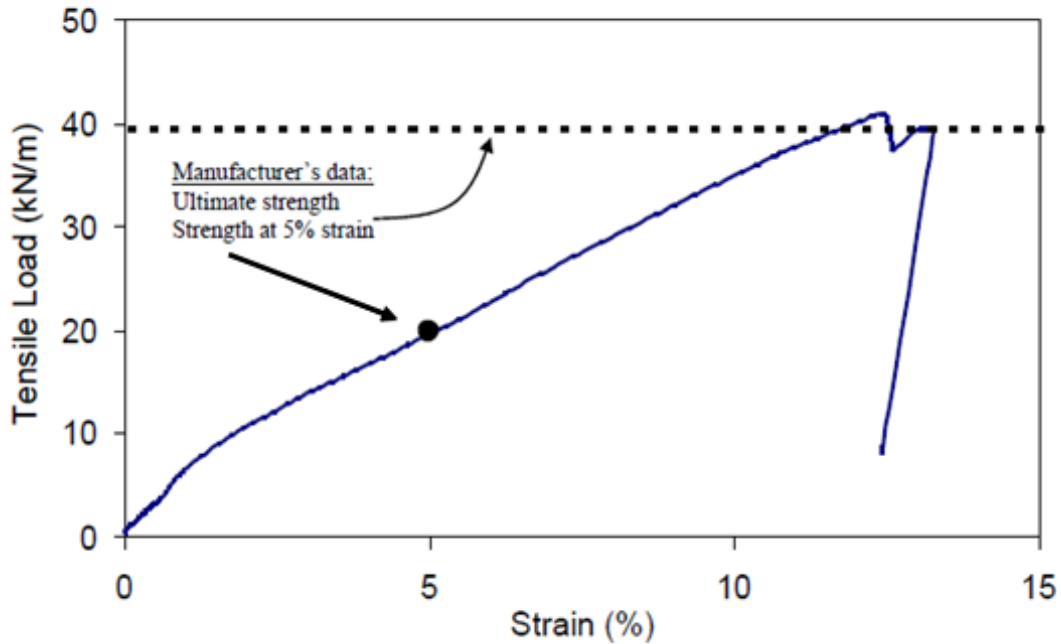


Figure 9. Mechanical response of the geotextile used in the pullout tests (Mirafi HP370) as per the ASTM D4595 test protocol and as compared with the manufacturer's data (Hatami et al. 2010a). Note: The two arrows show the 5%-strain and ultimate tensile strength values of the geotextile reinforcement (1 kN/m = 68.5 lbs/ft)

## 6. REDUCED-SCALE EMBANKMENT TESTS

### 6.1 METHODOLOGY

The model embankments were constructed and surcharge load tested at three different GWC values equal to OMC-2%, OMC and OMC+2% (Table 2). The differences in the magnitudes of the soil-geotextile interface strength and soil shear strength among these test cases were used

to determine a moisture reduction factor [MRF =  $\mu(\omega)$ ] as per Equations 3 and 4 to account for the loss of reinforcement pullout resistance and interface shear strength due to increased GWC value in the soil.

Table 2. Test information for reduced-scale reinforced embankments

<b>Test information</b>	
<b>Soil</b>	Silty clay
<b>Geosynthetic reinforcement</b>	Mirafi HP370, woven PP
<b>Moisture content</b>	OMC-2%, OMC, OMC+2%

### 6.1.1 Test Equipment

A 6.5 ft (L) × 2.5 ft (W) × 4ft (H) portable embankment test box with an integrated loading frame was fabricated for the tests carried out in this study. In this configuration, the self-reacting loading frame of the test station was mounted on the test box itself as opposed to the strong floor (Figure 10). A main advantage of this design was that the test station would not be restricted to any particular location within the laboratory where a strong floor would have to be available. In addition, the loading frame was designed so that it could be mounted on the top of the test box at several designated locations to allow for flexibility in testing scenarios in the current and future projects. The sidewalls of the test box were lined with of 1¼-in.-thick polycarbonate glass panels so that the embankment deformations (including the formation of slip plane) could be monitored and measured. The steel columns and the thickness of the polycarbonate glass panels were designed so that the sidewalls of the text box would be essentially rigid when the embankment models were subjected to surcharge loading.



Figure 10. Test box and self-reacting loading frame fabricated for the reduced-scale reinforced embankment tests in this study

Prior to the laboratory tests, numerical models of the 3.2 ft-high embankments were analyzed using the computer program FLAC v. 5.0 (Itasca 2005) to determine predicted magnitudes of failure loads and embankment deformations and to finalize their instrumentation layout. The shear strength properties of the soil in the modeled embankments were varied based on their GWC values for different test cases as shown in Table 3. Current design guidelines of reinforced soil structures in North America use a  $70^\circ$  batter angle to separate steepened embankments from retaining walls (e.g. AASHTO 2008, Berg et al. 2009). Therefore, in this study, the model embankments were constructed with a target slope angle value of  $69.5^\circ$  in order to avoid a prohibitively long test box and to represent the most critical geometry for the RSS structures (i.e. with the lowest factor of safety and largest expected deformations). It would also help ensure that the box deformations during the surcharge loading phase of the tests remained negligible before the embankment models failed.

Table 3. Material properties used in FLAC simulations

<b>Test cases</b>	<b>OMC-2%</b>	<b>OMC</b>	<b>OMC+2%</b>
<b>Soil density (lb/ft<sup>3</sup>)</b>	125.9	128.1	130.3
<b>Soil cohesion (psi)</b>	4.8	3.0	2.3
<b>Soil friction angle (°)</b>	35.3	34.2	34.0
<b>Soil-Geotextile adhesion (psi)</b>	2.6	1.8	1.7
<b>Soil-Geotextile interface friction angle (°)</b>	27.8	24.9	21.8
<b>Geotextile thickness (in.)</b>	0.035	0.035	0.035
<b>Geotextile tensile yield strength (lb/ft)</b>	2740	2740	2740

The preliminary numerical simulations shown in Figure 11 included an 8-in.-thick foundation zone at the bottom. However, the presence of such a layer proved to be inconsequential with respect to the magnitude of predicted failure load and the geometry of the failure plane. Hence, it was decided to construct the model embankments without the foundation layer to reduce the construction time. The surcharge load was applied as a line load across the length of the model embankment (i.e. along the running length of the slope) using a 4-in.-wide steel footing beam that was located at 12.5 inches from the crest of the embankment slope and was loaded with a 20-kip hydraulic actuator (Figure 8a). Figure 11 shows the failure surface for the slope embankment as predicted in one of the FLAC simulations.

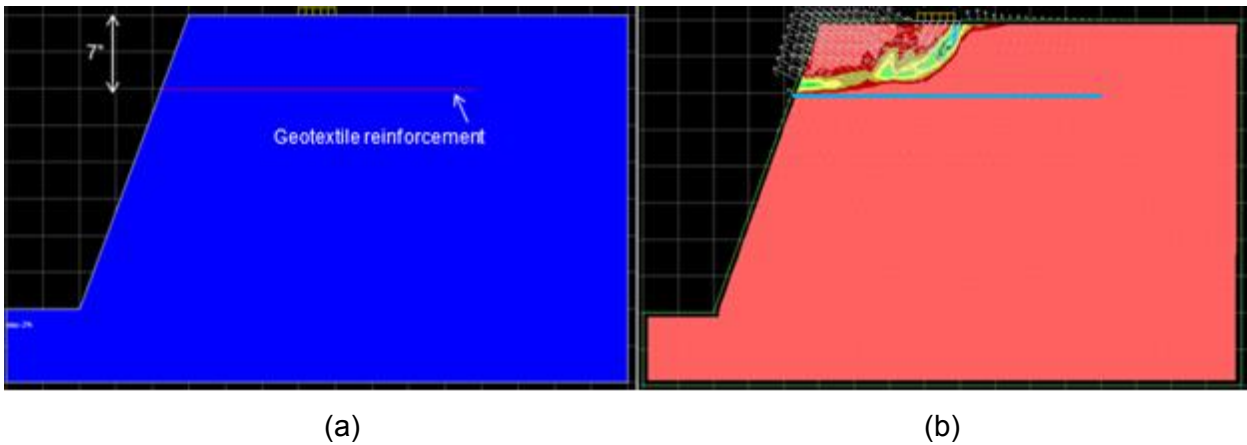


Figure 11. FLAC simulation of a reduced-scale reinforced embankment model; (a) Model at the end of construction, (b) Failure surface geometry in the embankment when subjected to strip footing load

## 6.2 TEST PROCEDURE

### 6.2.1 Soil Processing

After the soil was transported from the borrow site in CS 2780, Chickasha OK to the Fears lab at OU, the clayey soil was air dried and broken into small pieces. Afterwards, the soil was passed through a #4 sieve using a Royer shredder and sifter machine (Figure 12). Next, the soil was mixed with water to reach the target GWC value for each test (Figure 13a). The wet soil was stored in one hundred and forty (140) 55lb-buckets and was sealed for more than 24 hours to reach moisture equilibrium (Figure 13b). The soil gravimetric water content (GWC) in each bucket was measured using the oven drying method. The above procedure was repeated for every test.



Figure 12. Soil processing for reduced-scale embankment tests using a crusher-sifter machine



(a)



(b)

Figure 13. Soil mixing; (a) Mixing of soil to reach target gravimetric water content, (b) Sealed buckets containing processed soil before constructing the model embankment in the test box

## 6.2.2 Construction of Model Embankments

Before constructing the model embankments in the test box, its side walls were lined with thin clear sheets of plexiglass to protect the polycarbonate glass panels against scratches during soil placement and compaction. Next, the soil was placed and compacted in the test box in five 4-inch lifts followed by nine two-inch lifts. Preliminary testing and numerical simulation had indicated that the geometry of the failure plane would be contained within the upper half of the embankment models which would also exhibit significantly larger deformation as compared to its lower region. Therefore, the bulk of the instrumentation was concentrated over the upper half of the embankment models (Figure 8a). This allowed the bottom half of the embankment models to be constructed with larger lifts to expedite the otherwise time-consuming construction process without adversely impacting the performance of the model embankments relative to the study objectives. The soil was compacted to 85% and 95% of its maximum dry unit weight (i.e.  $\gamma_d = 120 \text{ pcf} = 18.8 \text{ kN/m}^3$ ) within the four-inch and two-inch lifts, respectively (Figure 8a). The compaction for each layer took approximately 2 hours.

The sensors were placed in the embankment based on the instrumentation plan shown in Figure 8. The instrumented geotextile layer was placed 7 inches below the embankment surface. The test box containing compacted soil at its target gravimetric water content was sealed with plastic sheets on the top (Figure 14a). Afterwards, the facing slope was trimmed to complete the construction stage before the model was subjected to surcharge loading (Figure 14b). Furthermore, prior to the loading stage, the constructed embankment was left in sealed condition for a few days until the EC-5 and PST-55 psychrometer sensors reached equilibrium with their surrounding soil and the gravimetric water content within the embankment stabilized.(d)

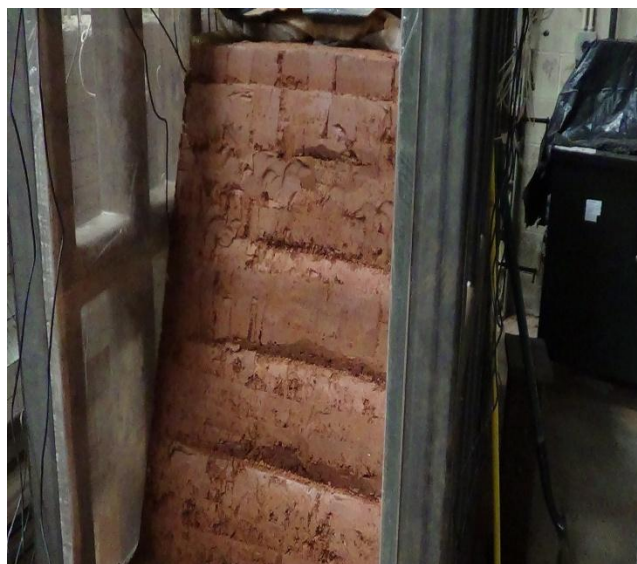
Figure 23. Displacements recorded during the embankment tests; (a) Lateral displacement of the test box near the top of the embankment (Figures 8a and 15b), (b) Vertical displacement of the embankment near the footing, (c) Horizontal displacement of the embankment's facing for the test case at OMC-2%, (d) Horizontal displacement of the embankment's facing for the test case at OMC

15 shows the locations of the 5 LVDTs that were mounted on the embankment and test box based on the instrumentation plan shown in Figure 8. Please note that two more vertical LVDTs installed on the embankment's surface (i.e. near footing) and one more horizontal LVDT mounted on the test box are not shown in Figure 15.

Three (3) earth pressure cells (EPC) and twenty four (24) tactile pressure sensors were used in the model embankments to monitor earth pressure at different locations during surcharge loading phases of the tests (Figure 8). One EPC sensor was installed vertically against a polycarbonated glass sidewall to measure the soil lateral pressure on the wall of the test box (Figure 19).



(a)



(b)

Figure 14. Embankment construction; (a) Sealing of model embankment during construction to preserve its water content, (b) Trimmed front facing of the model embankment before applying the footing loading on the top



(a)



(b)

Figure 15. Locations of LVDTs for the reduced-scale embankment tests; (a) LVDTs to measure embankment deformation, (b) LVDTs to measure test box deformation

### 6.2.3 Loading of Model Embankments and Dismantling of the Test Setup

The loading phase of the embankment tests typically took between 6 and 10 hours depending on the gravimetric water content of the embankment soil. The strip footing was placed on the embankment 12.5 inches away from the embankment crest (Figure 8a). The bottom of the footing was covered with sandpaper to simulate a rough counterface (e.g. a concrete bridge abutment). A 50-kip, 6-inch stroke hydraulic cylinder (Enerpac Model 506) was used to apply a vertical line load on embankment via the strip footing. It was made sure that the hydraulic cylinder was placed precisely at the center of footing and the reaction beam to avoid unexpected tilting of the strip footing (Figure 16). The vertical load was applied statically in 300 lb increments after it was observed at each load step that the rate of footing settlement had been reduced to less than 0.002 in/min following the application of the load. The loading continued until a clear and continuous failure surface was started from the top of the embankment and extended to the slope.

Figure 17 shows the slip surface for the test with the embankment constructed at OMC-2%. After the test was completed and the embankment failed, the test assembly was carefully dismantled. First, the surcharge assembly was removed from the top of the box and the soil in

failure zone was carefully excavated out of the box (Figure 17b). It typically took between 8 and 10 hours to carefully dig the entire soil out of the test box and remove all the sensors buried within the embankment. Altogether, a complete test required approximately 65 to 70 hours of hands-on operation including processing and mixing of the soil, construction and instrumentation of the model embankment in the test box, 36 to 48 hours as equilibrium time for moisture and suction sensors and 8 to 10 hours to run the surcharge loading test.

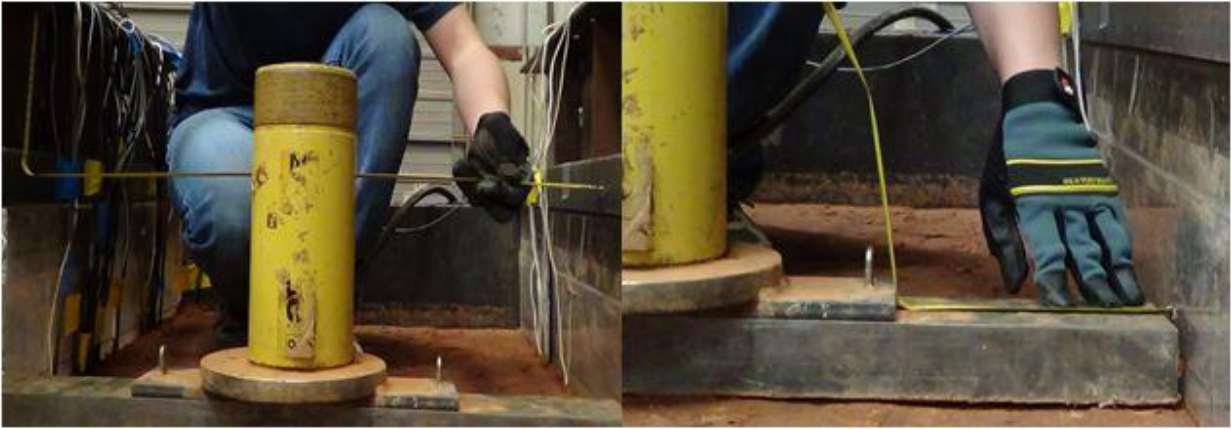
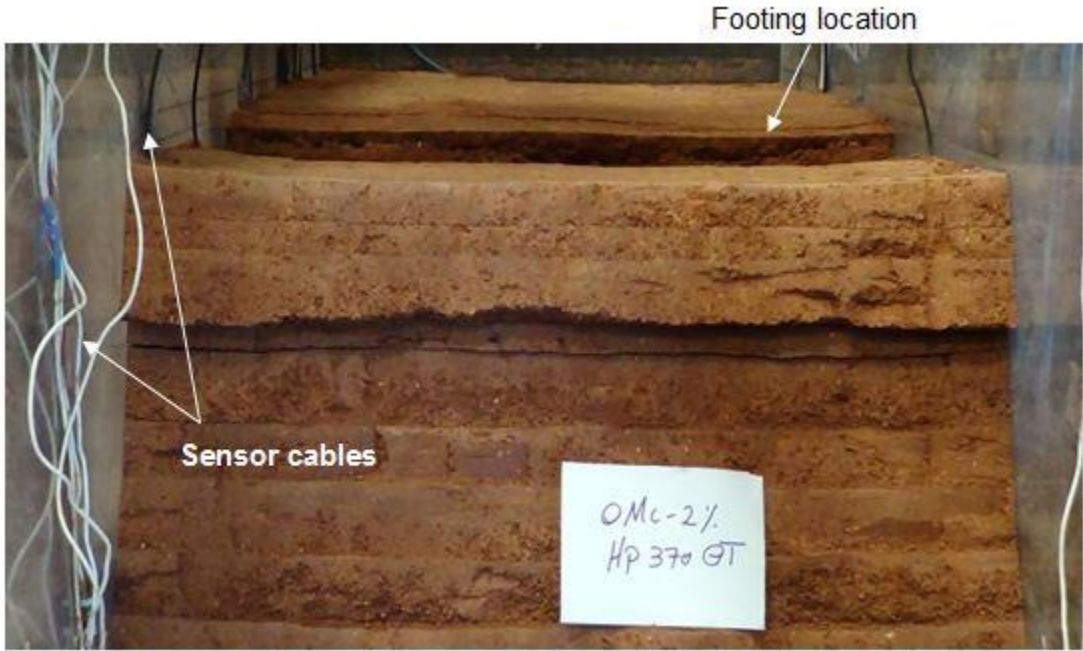
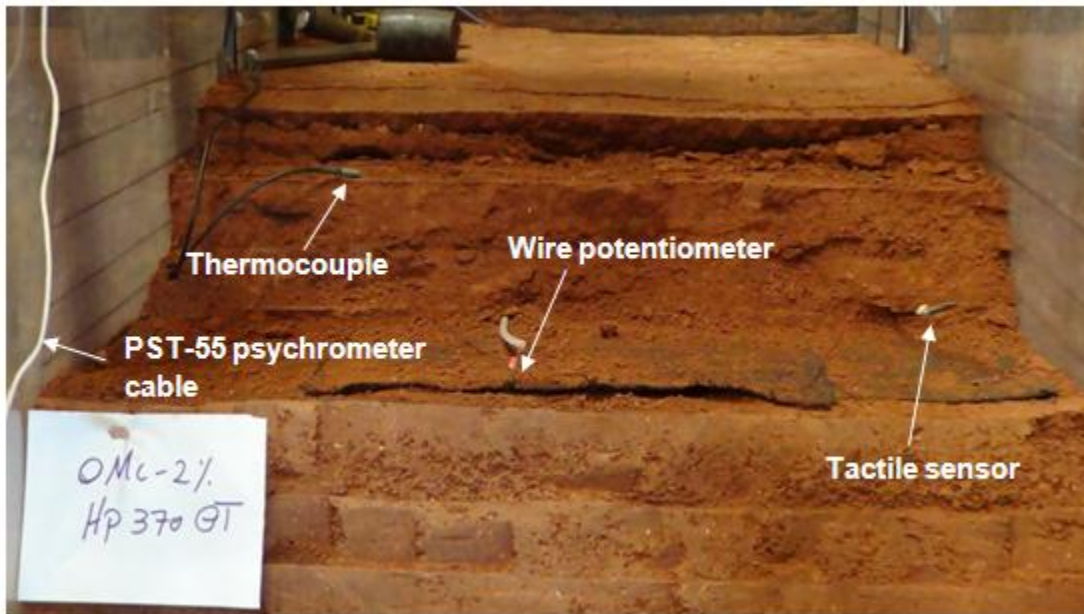


Figure 16. Placing the hydraulic cylinder at the center of footing and reaction beam in embankment tests



(a)



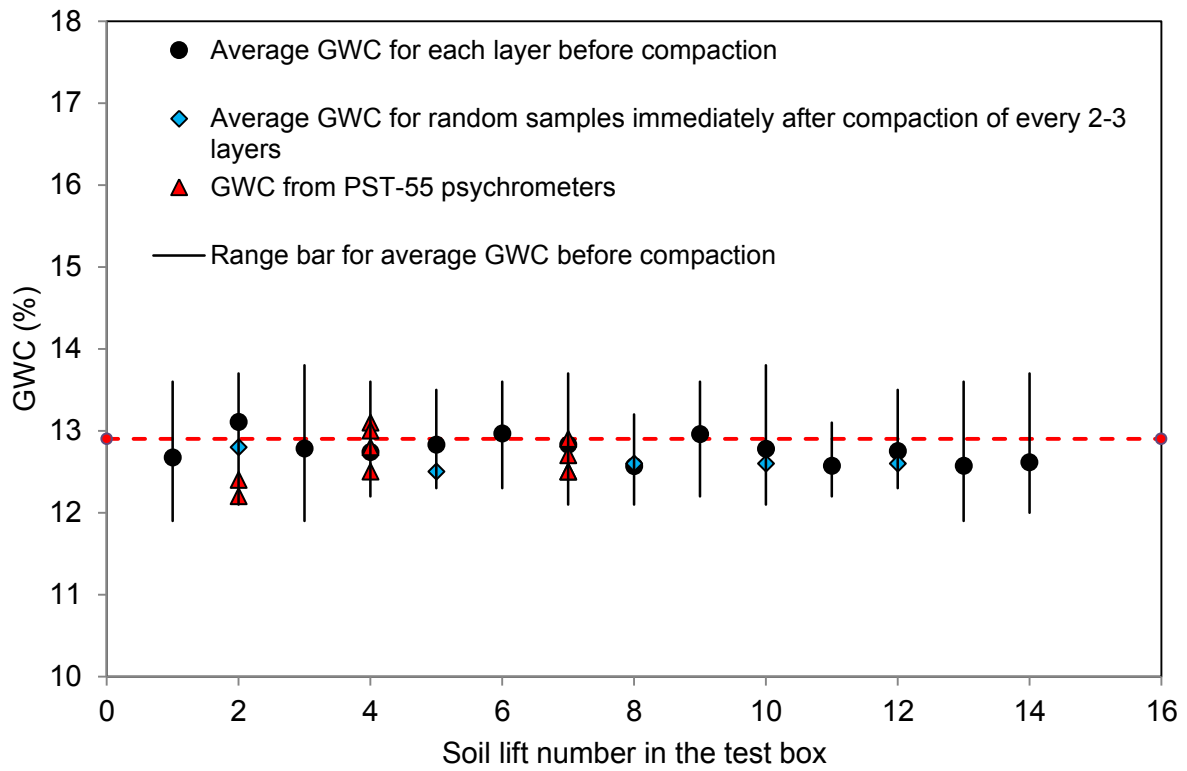
(b)

Figure 17. Failure surface after surcharge loading in the model embankment constructed at OMC-2% with woven geotextile HP370; (a) Before excavation, (b) After excavation of failure wedge

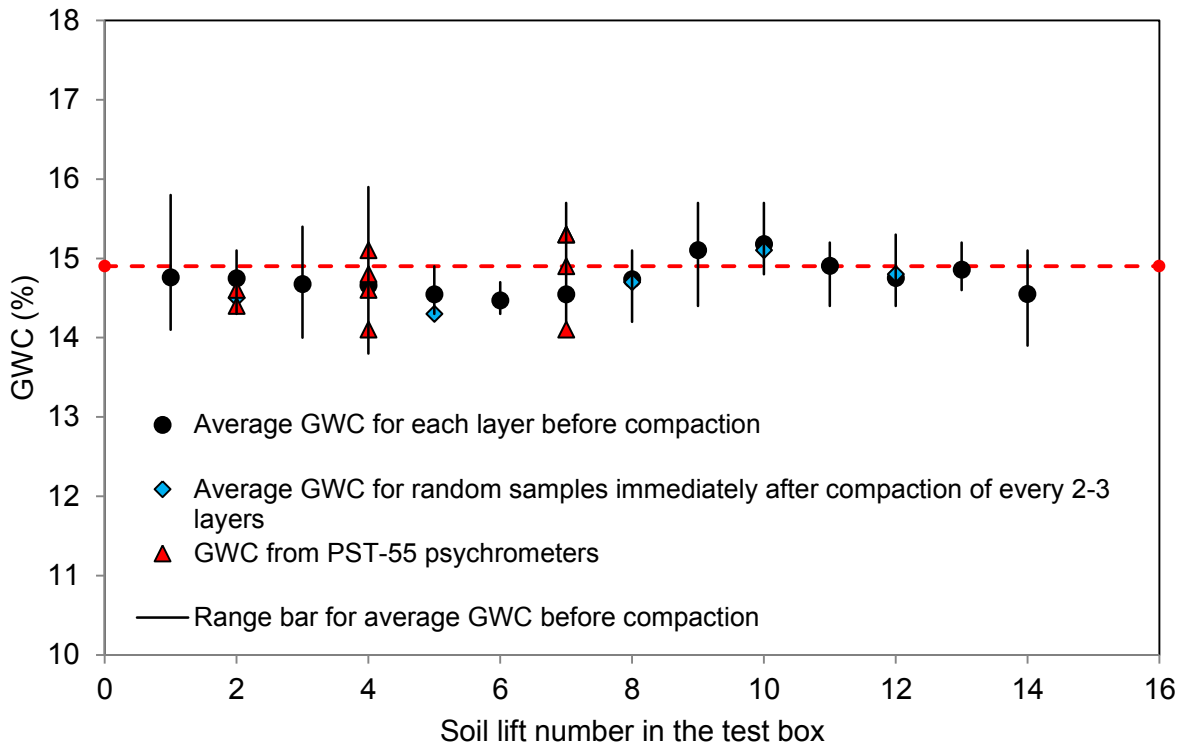
#### 6.2.4 Soil Gravimetric Water Content and Suction

During construction of each embankment model, the GWC value of each soil lift was determined by taking 6 soil samples during compaction using the oven drying method (ASTM 2216-10). In addition, random soils samples were taken (on the order of 3 from the surface of the soil after each 2-3 layers had been compacted) to measure their GWC values and make sure that the loss of soil water content as a result of the compaction procedure was negligible. Figure 18 shows the distributions of the soil water content within the embankment for all test cases carried out in this study. The results are compared with the GWC values obtained from the SWCC (Figure 6) and PST-55 psychrometers to examine how close the as-placed values were to the target values.

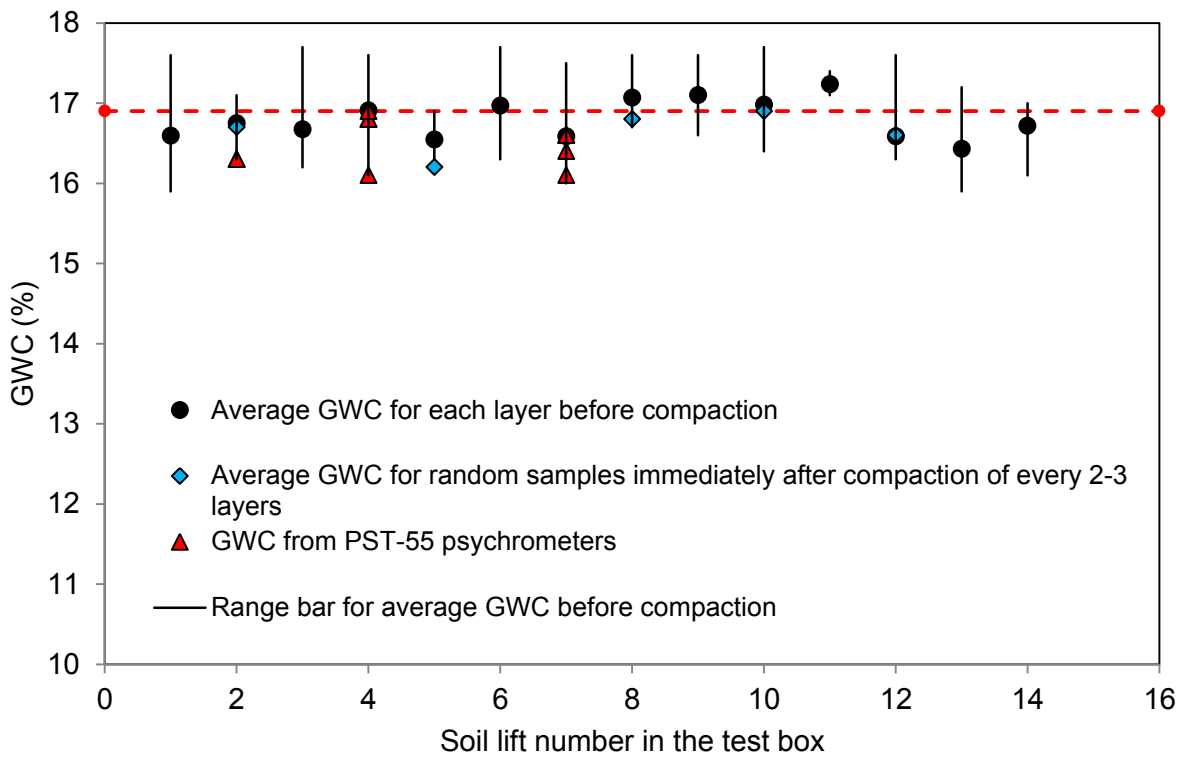
The EC-5 sensors were also used to monitor the soil water content in the embankments before and after the tests. However, they were only used at the end of construction to find out when the water content in the embankment stabilized before the embankment could be loaded (Figure 19). Figure 20 shows the data from EC-5 sensors versus time, which indicate that the GWC within the embankment had been stabilized before the loading tests started.



(a)



(b)



(c)

Figure 18. GWC data within the embankment from oven-drying method and PST-55 psychrometers; (a) Test case at OMC-2%, (b) Test case at OMC, and (c) Test case at OMC+2%. Notes: <sup>(1)</sup> Red dashed line shows the target GWC value, <sup>(2)</sup> Six (6) samples were taken from each layer to determine an average GWC value before compaction, <sup>(3)</sup> Three (3) random samples were taken immediately after compaction of 2-3 layers of embankment

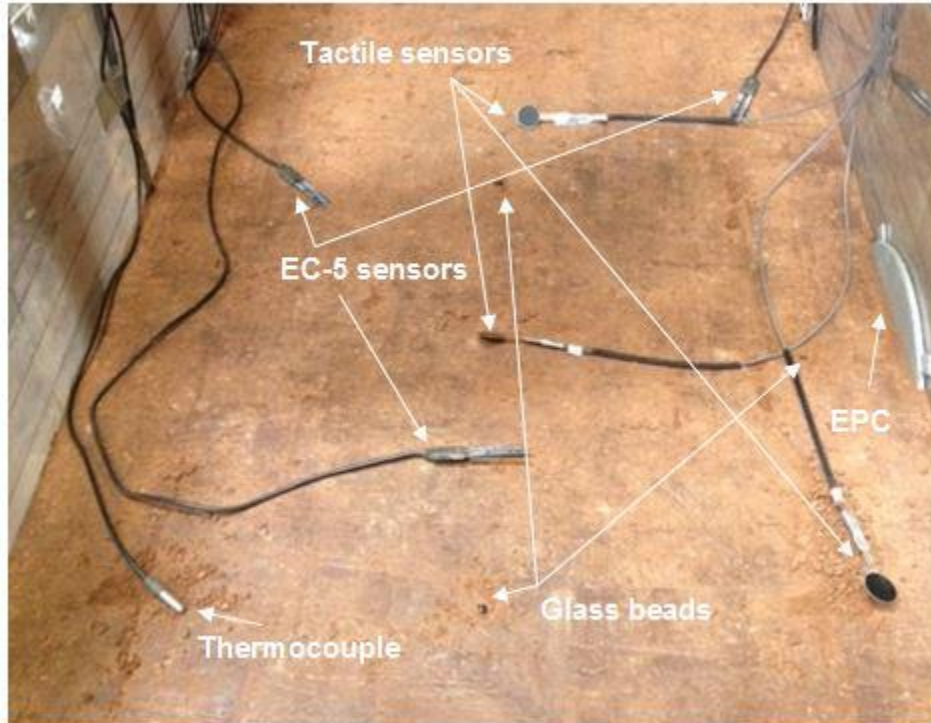
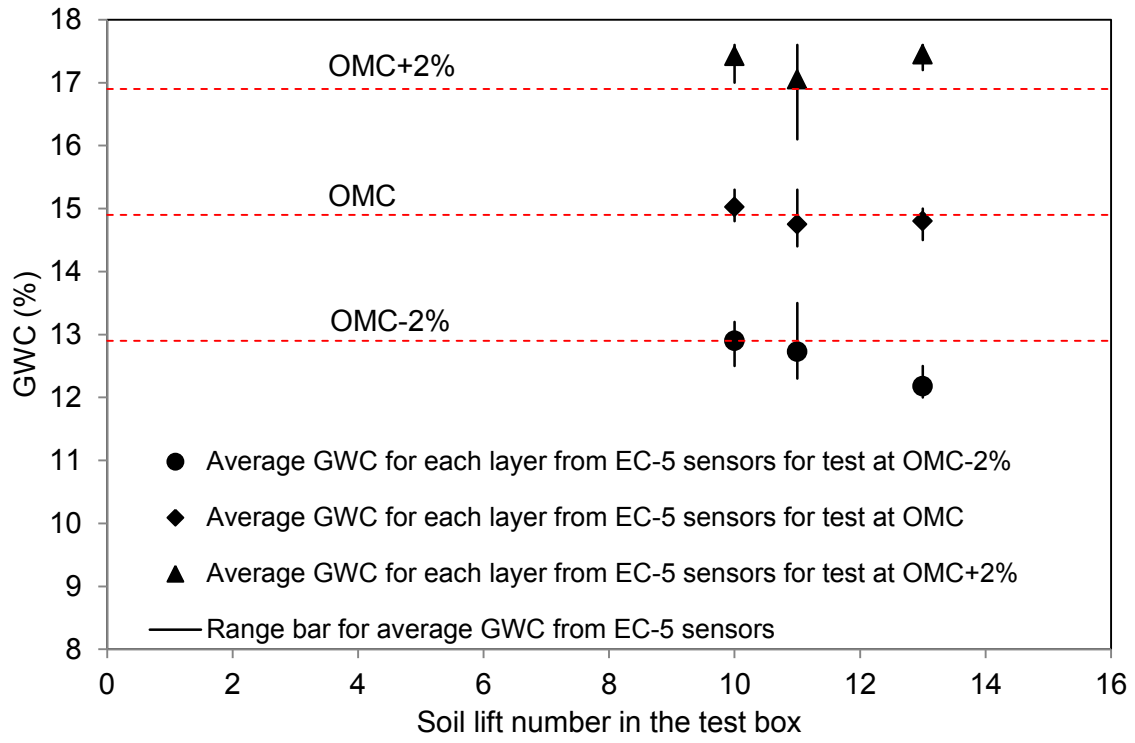
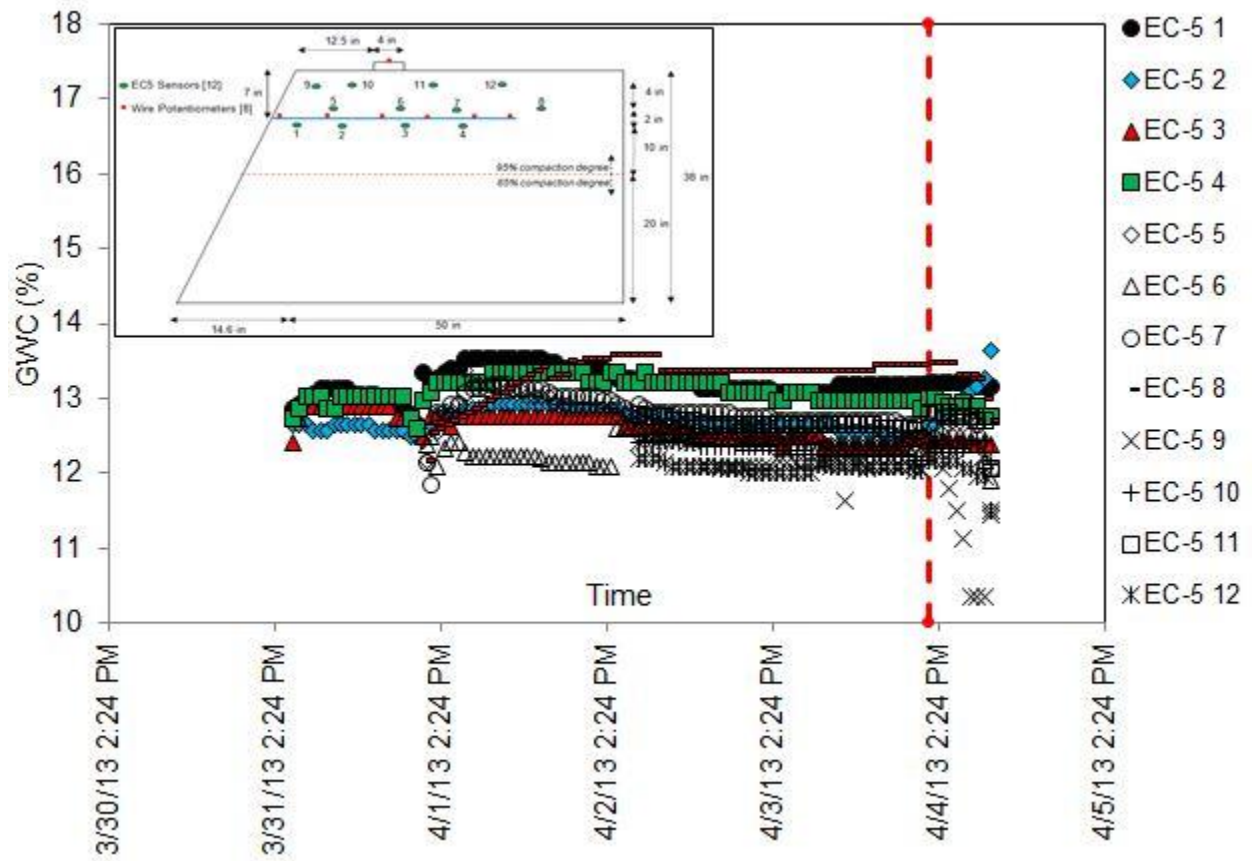


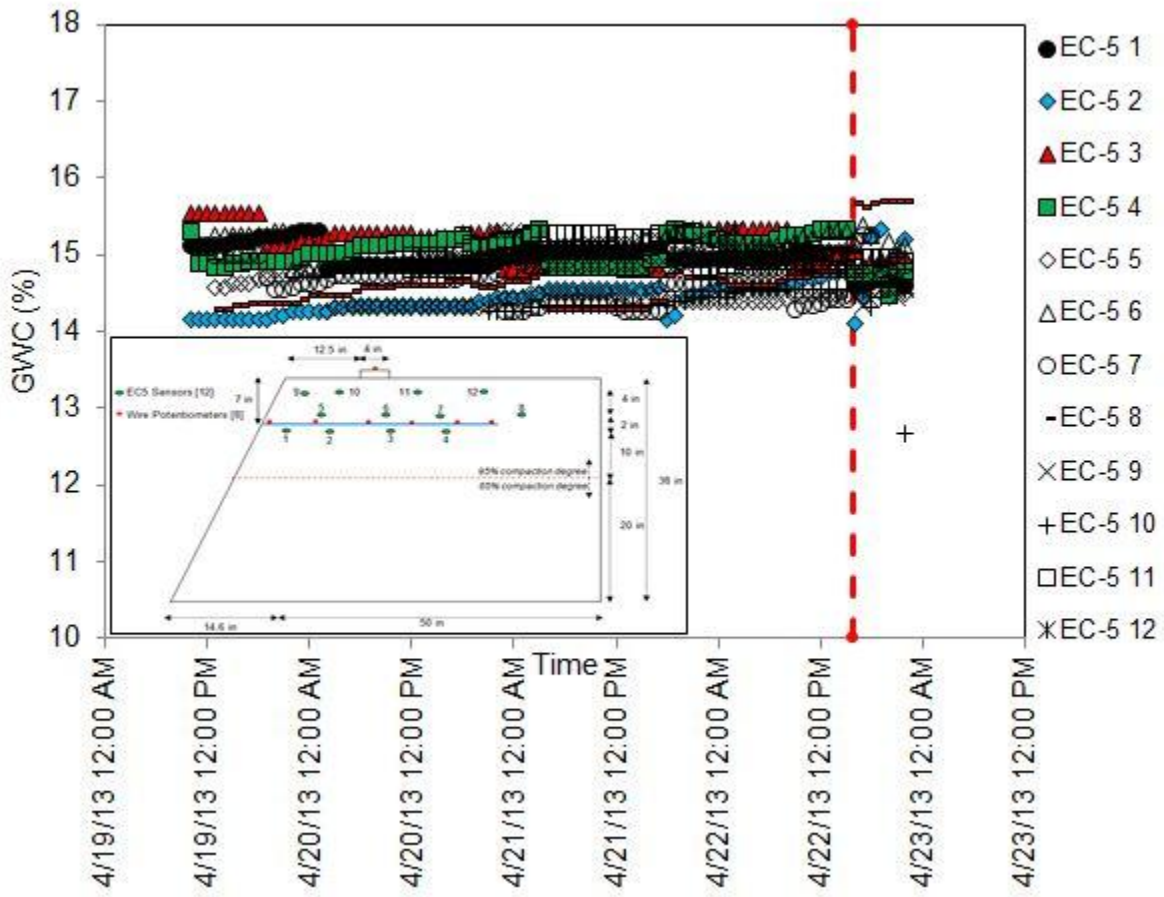
Figure 19. Placement of the sensors before compaction of the layer



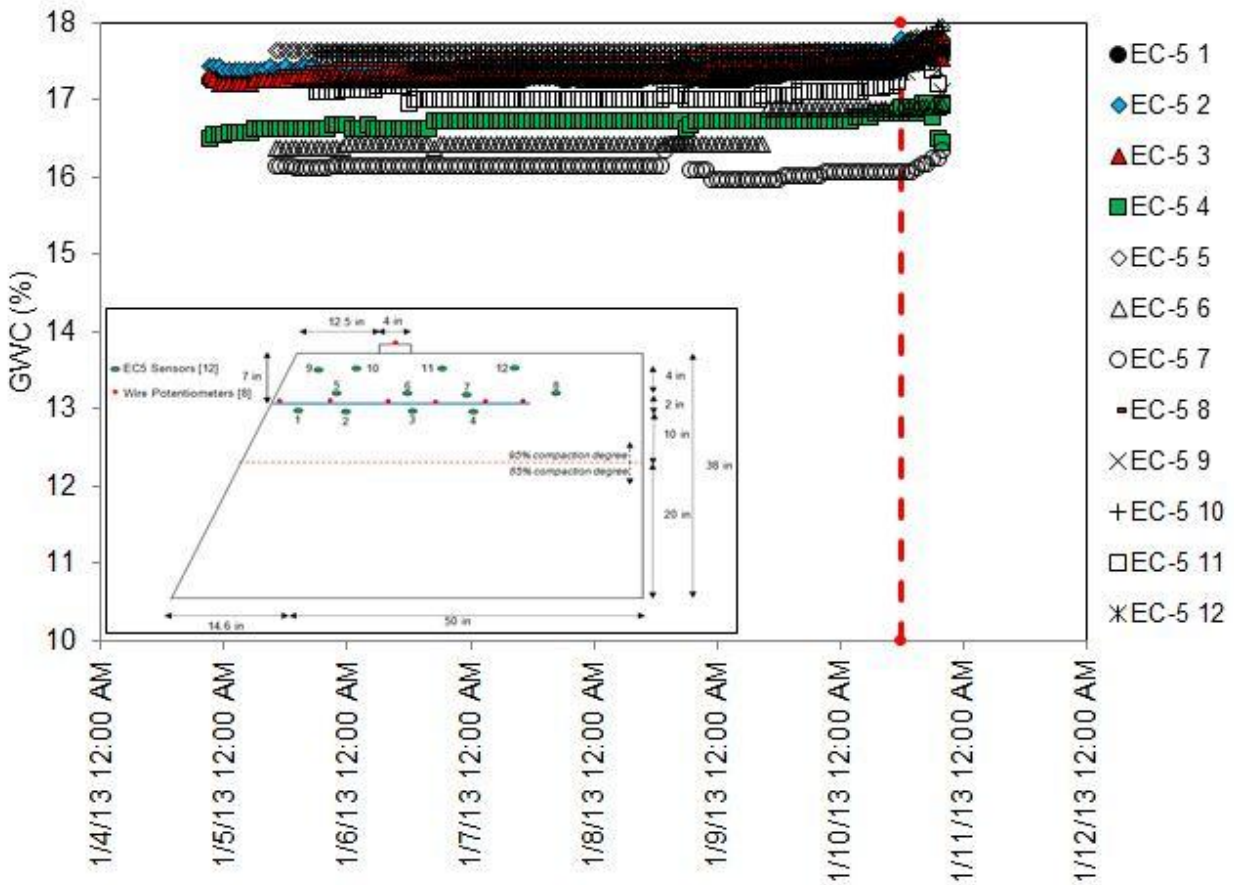
(a)



(b)



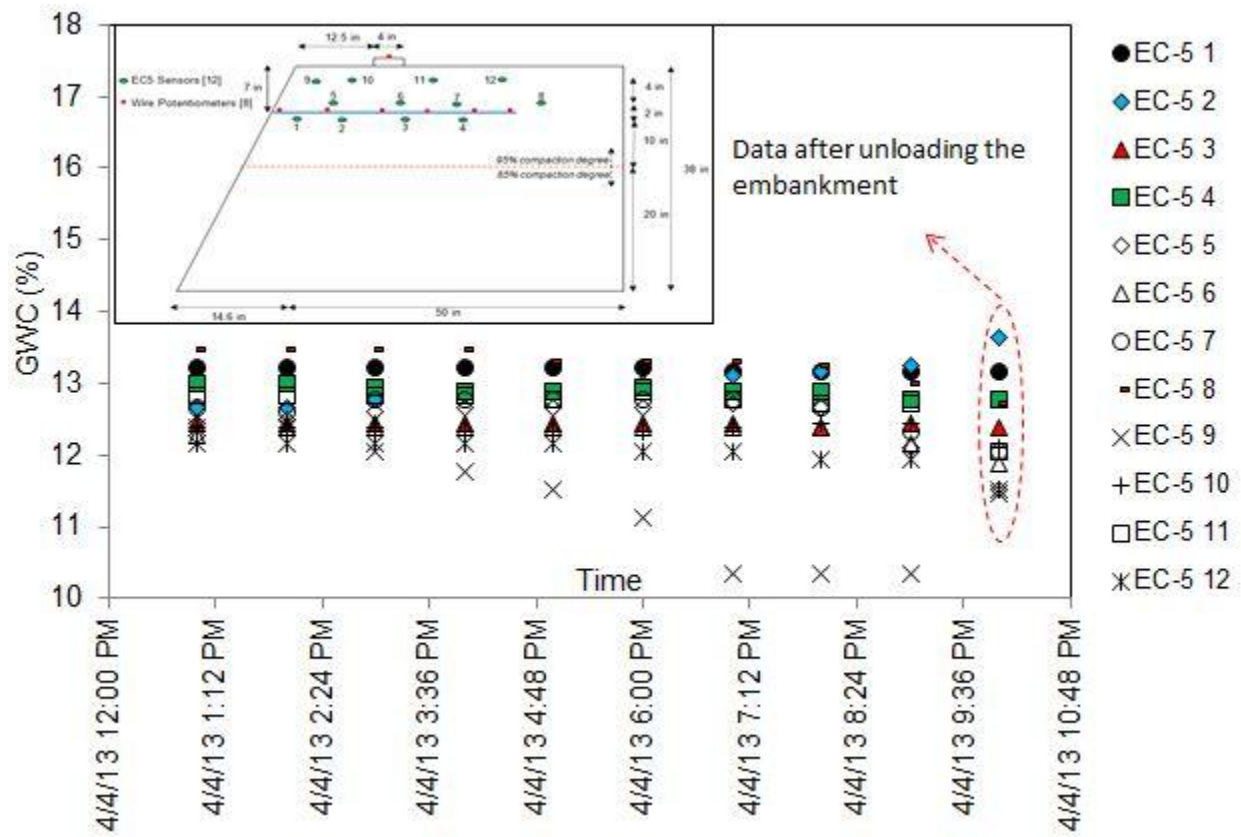
(c)



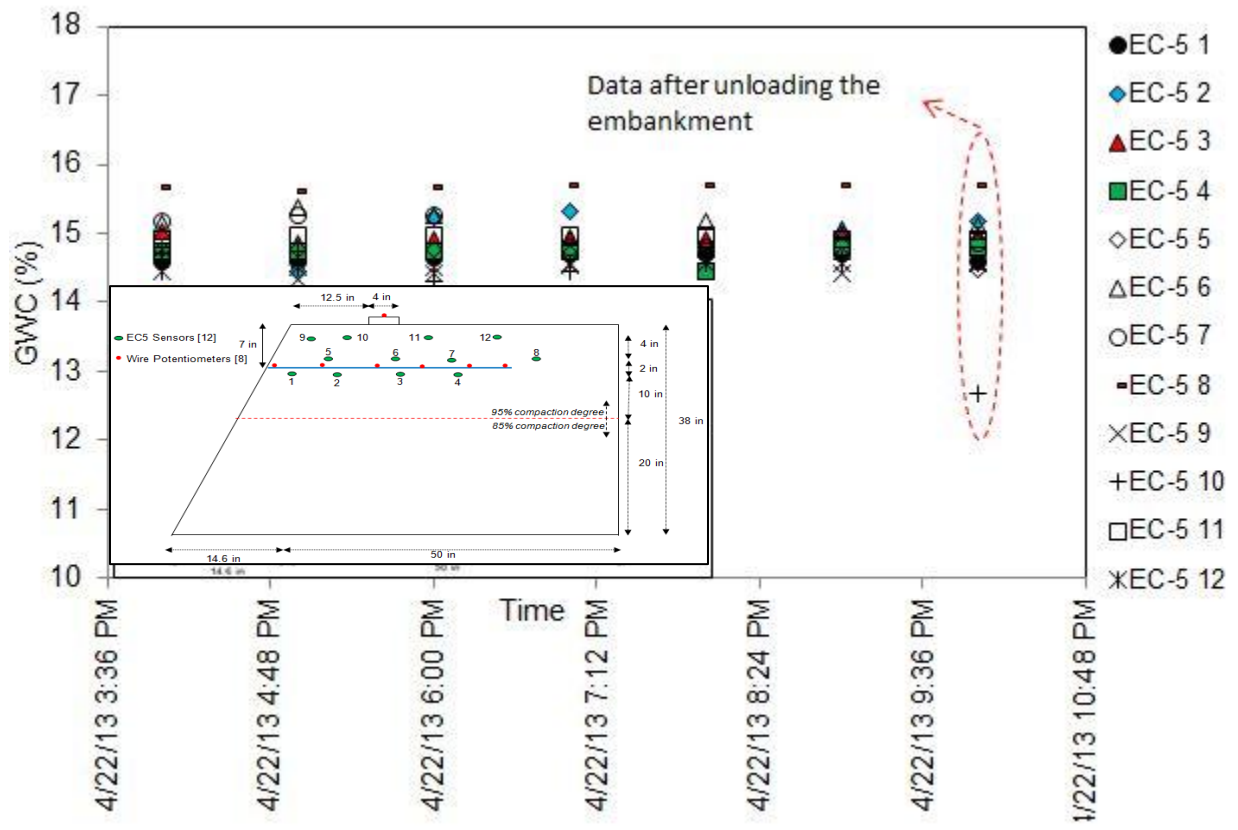
(d)

Figure 20. GWC data from EC-5 sensors in model embankments constructed at different GWC values; (a) Average GWC for each layer from EC-5 sensors at the end of construction (b) OMC-2%, (c) OMC and (d) OMC+2%. Note: The vertical red dashed line indicates the time when the loading started

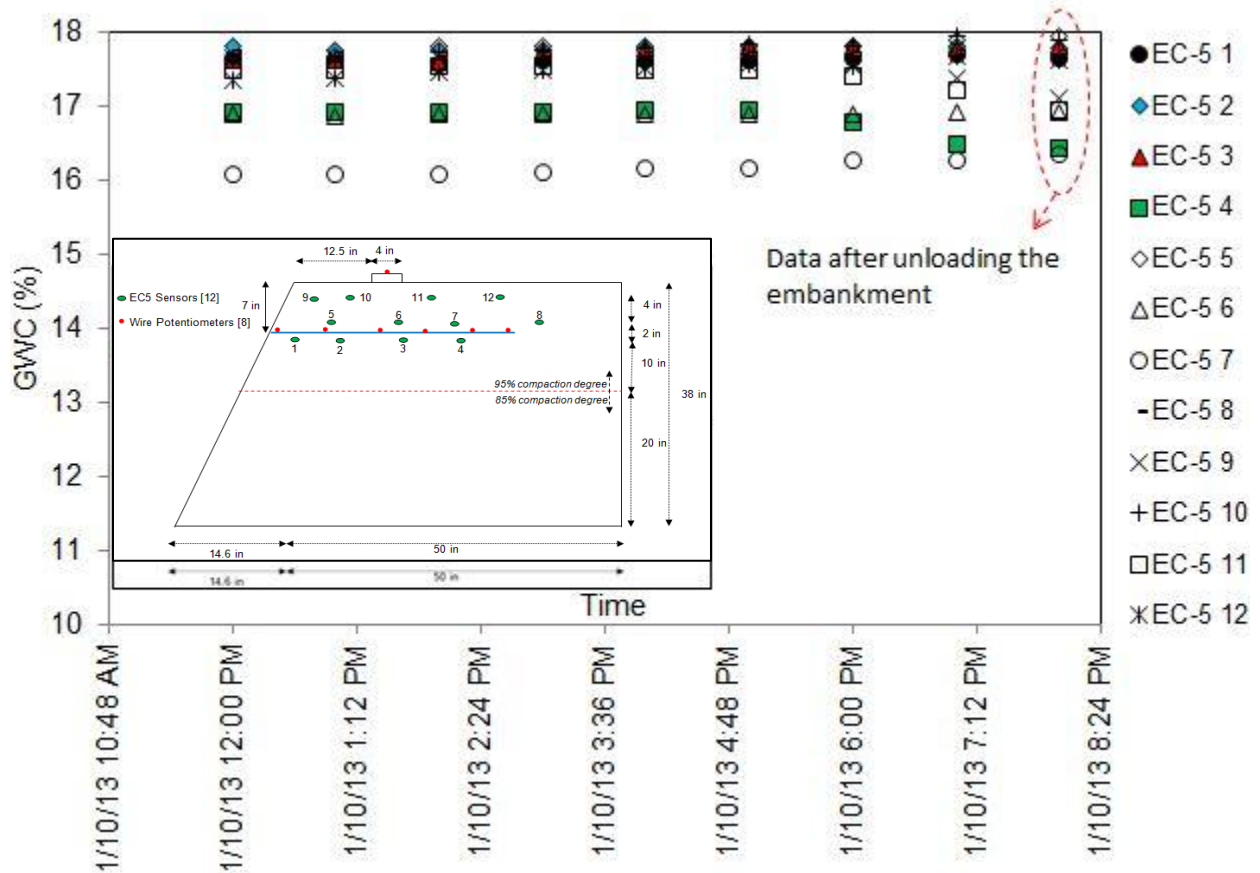
Figure 21 shows the GWC values in the embankment as monitored with the EC-5 sensors during the loading stage of the tests. The results show that the soil water content in the model embankments remained essentially constant for nearly all cases except for the EC-5 9 at the OMC-2% test case. For the test at OMC-2%, EC-5 results show that the soil GWC in the embankment decreased after it was loaded for 3 hours. As is shown in Figure 21, EC-5 9 was located near the facing and the top surface of the embankment. Since setting up the LVDTs, footing and the load cell took longer than usual for the test at OMC-2%, the soil around EC-5 9 was drier the during surcharge loading stage than in other test cases. The last GWC readings from EC-5 sensors were taken during the unloading stage.



(a)



(b)

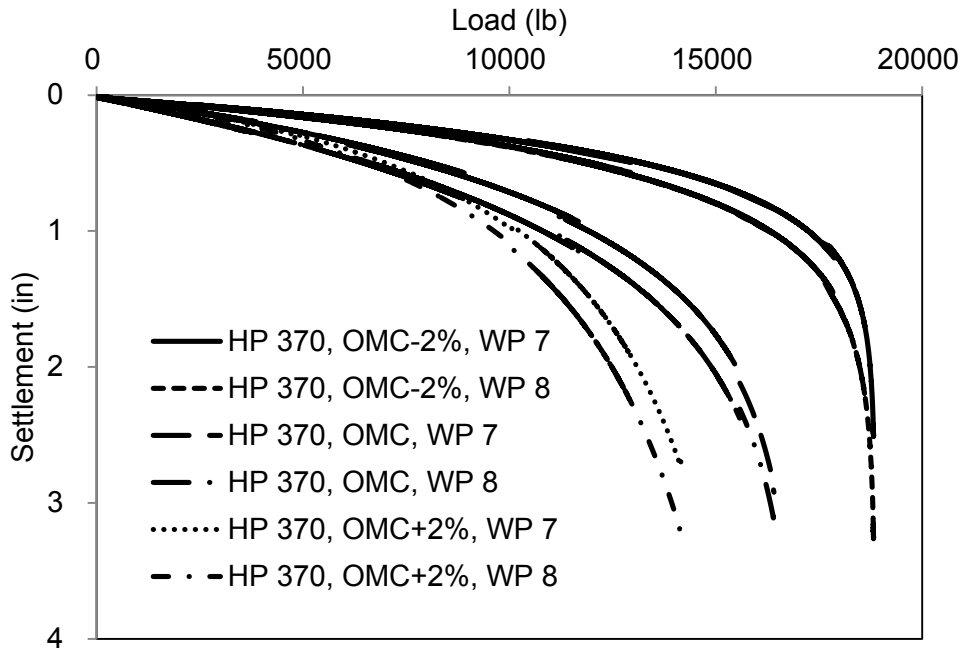


(C)

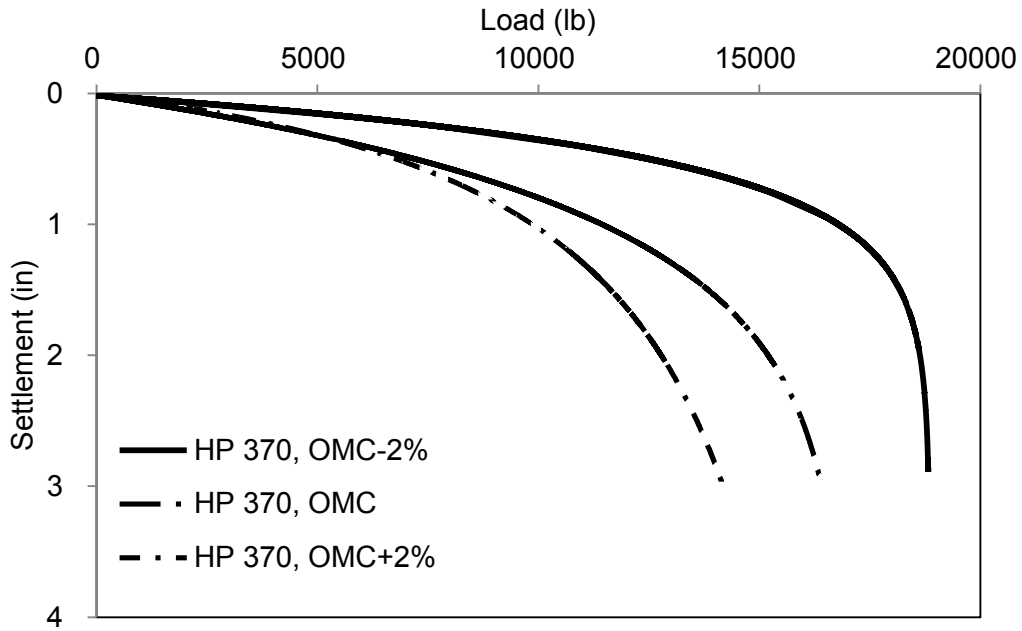
Figure 21. GWC monitored using EC-5 sensors after construction and during loading; (a) OMC-2%, (b) OMC and (c) OMC+2%

### 6.2.5 Load-Settlement Data

Figure 22 shows the load-settlement data for all three embankment tests. The measured compression load is plotted as a function of the strip footing settlement. Results in Figure 22 show consistently higher footing bearing capacity in the soil at OMC-2% as compared to the values in the OMC and OMC+2% cases. As expected, increasing suction led to a higher soil bearing capacity in otherwise identical embankment models.



(a)



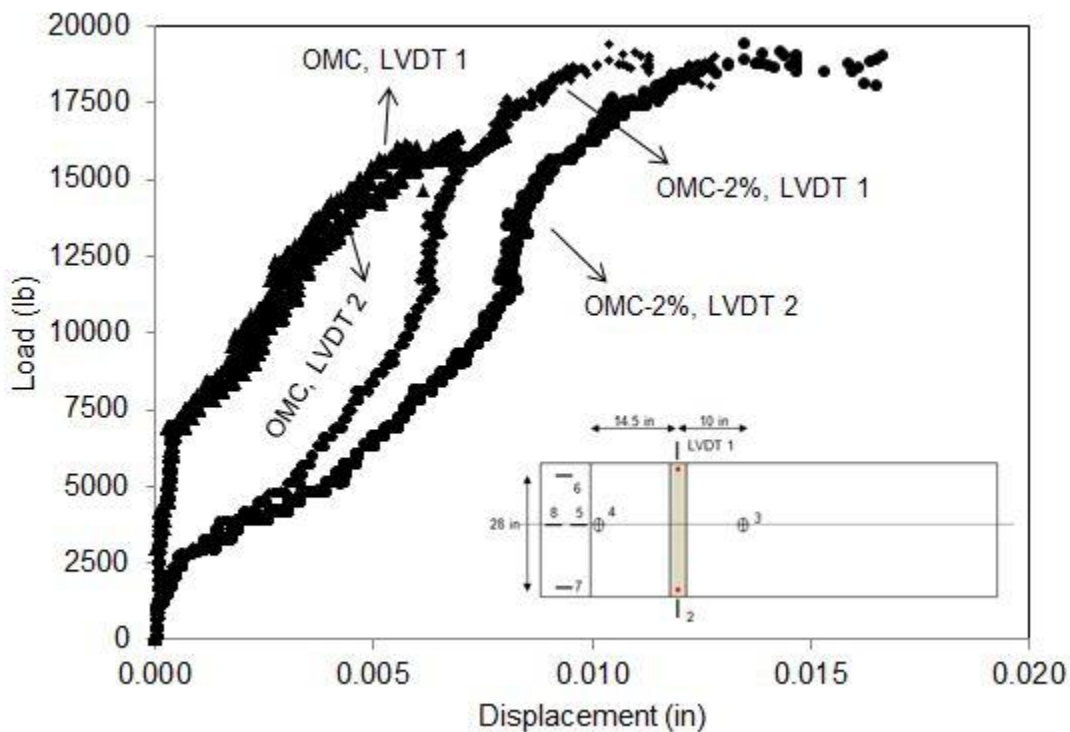
(b)

Figure 22. Load- settlement data for test soil at different GWC values (OMC-2%, OMC, OMC+2%); (a) Individual settlement recorded by WP 7 and WP 8, (b) Average of settlement values from WP 7 and WP 8

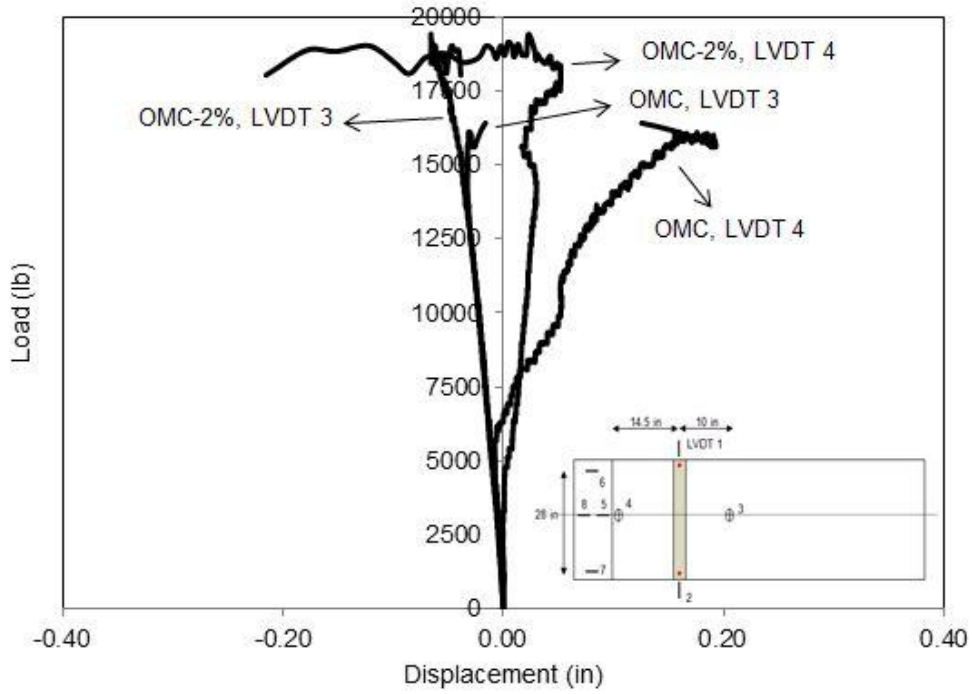
Results in Error! Reference source not found. 22 show the footing settlement readings from wire potentiometers WP 7 and WP 8 (Figure 22a), which were installed near the two ends of the footing (Figure 8b) and their average values (Figure 22b).

Figure 23a indicates that the maximum displacement of the test box's side wall which is for the test case at OMC-2% is negligible (i.e.0.015 inch) and validate the assumption of rigid side boundaries for the tests. The results in Figure 23a also show that the test box performed almost symmetrically while tests since the values recorded by LVDTs 1 and 2 are close to each other (The difference between LVDT 1 and 2 is less than 0.004 inch, depending on the test cases).

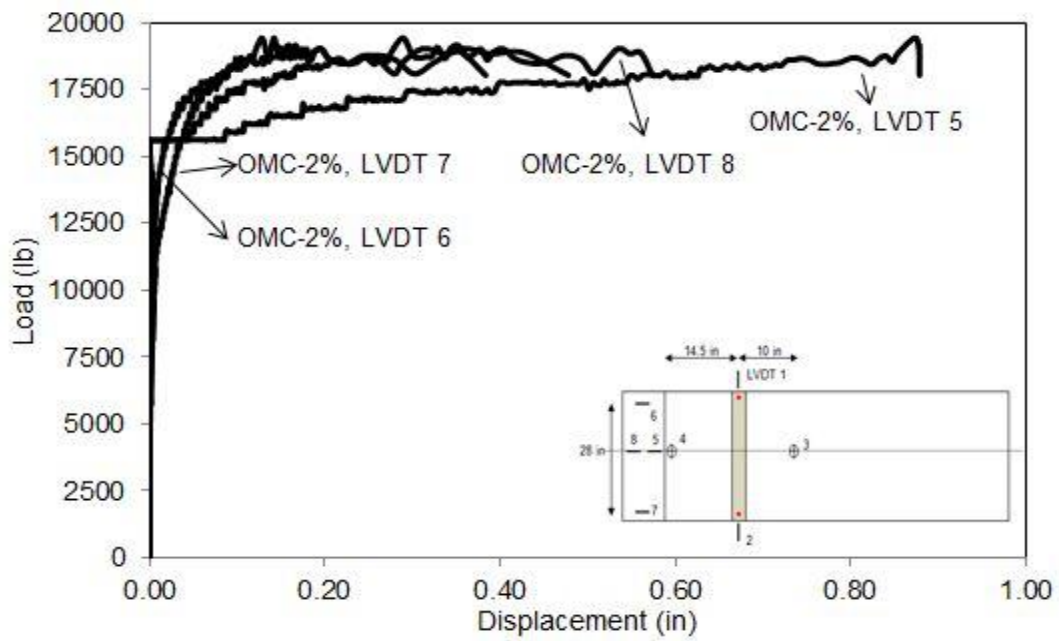
Figures 23b, c and d show the displacement values for the surface of the embankment in the vicinity of the footing and the facing while the embankments were loaded. Please refer to Figure 8 for the location of LVTDs. Results in Figures 23b indicate that the soil at the back of footing where LVDT 3 was installed settled before the failure reached in embankment and started to dilate around the ultimate load.



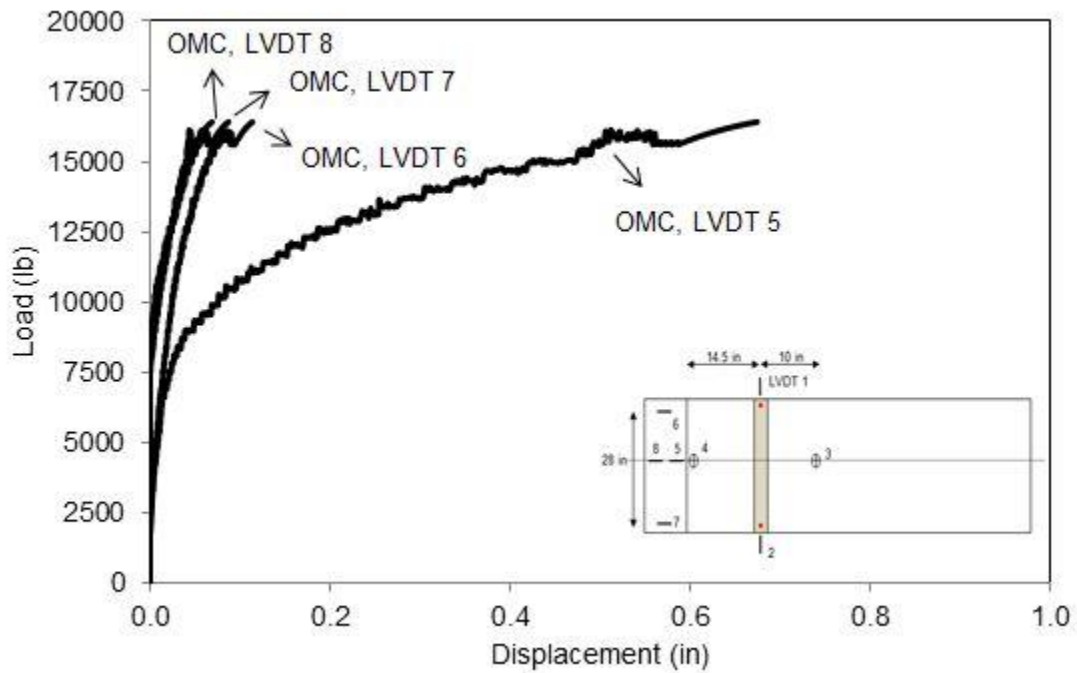
(a)



(b)



(c)



(d)

Figure 23. Displacements recorded during the embankment tests; (a) Lateral displacement of the test box near the top of the embankment (Figures 8a and 15b), (b) Vertical displacement of the embankment near the footing, (c) Horizontal displacement of the embankment's facing for the test case at OMC-2%, (d) Horizontal displacement of the embankment's facing for the test case at OMC

LVDT 4 was used to record the crest vertical movement in the model embankments. LVDT 4 results in Figure 23b indicate that the embankment crest started to heave once the embankment was subjected to the vertical loading of the strip footing 12½ inches away from the crest. The heaving continued throughout the test but started to reverse into settlement when the embankment approached failure. In the embankment model constructed at OMC, the failure wedge developed immediately above LVDTs 6 and 7. In comparison, in the model built at OMC-2%, the failure occurred immediately below the same sensors. In all three tests, no detectable movements were observed in the coordinates of the glass beads that were embedded in the embankment models.

The readings from the EPC sensors readings are shown in Figure 24. The Boussinesq method (Budhu 2000) was used to compare theoretical predictions of the vertical and horizontal incremental stresses within the embankment due to a line loading (as given in Equations 7 and 8) with the measured values. With X, Y and Z representing the directions along the running length, width and depth of the model embankments, respectively, the incremental vertical stress in the soil is given by:

$$\Delta\sigma_z = \frac{2qz^3}{\pi(x^2+z^2)^2} \quad (8)$$

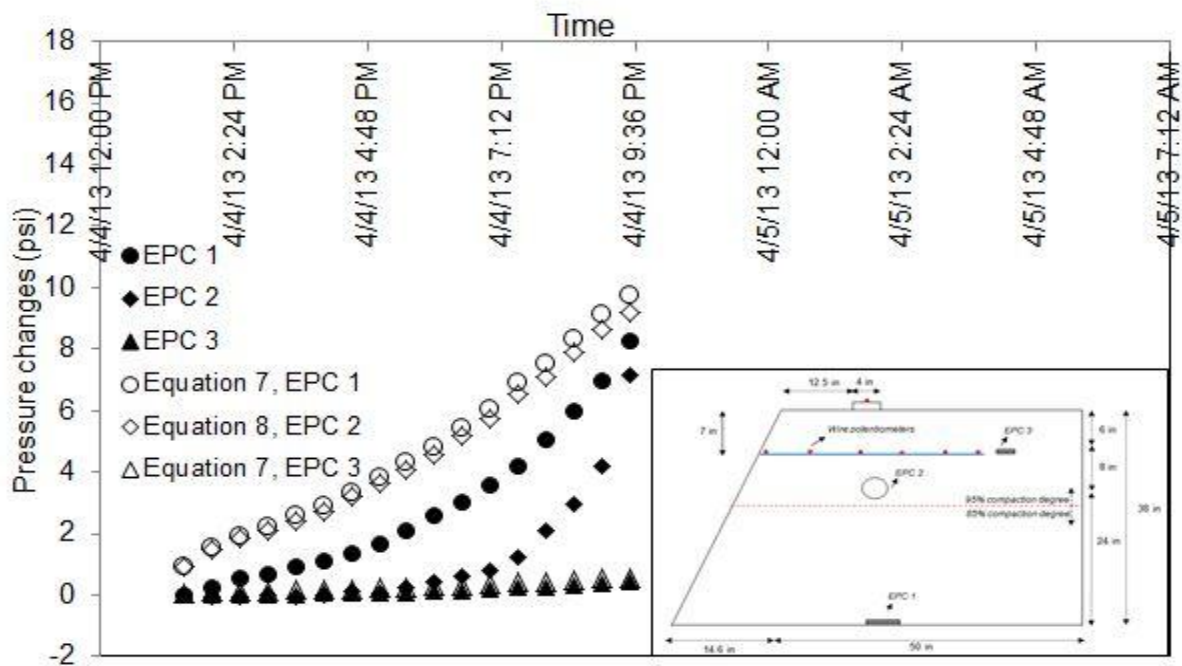
Where:

- i.  $\Delta\sigma_z$ : Increase in vertical stress
- ii. q: Vertical line load, lb/in
- iii. z: Vertical distance between the point the stress should be calculated and center of the line load
- iv. x: Horizontal distance between the point the stress should be calculated and center of the line load

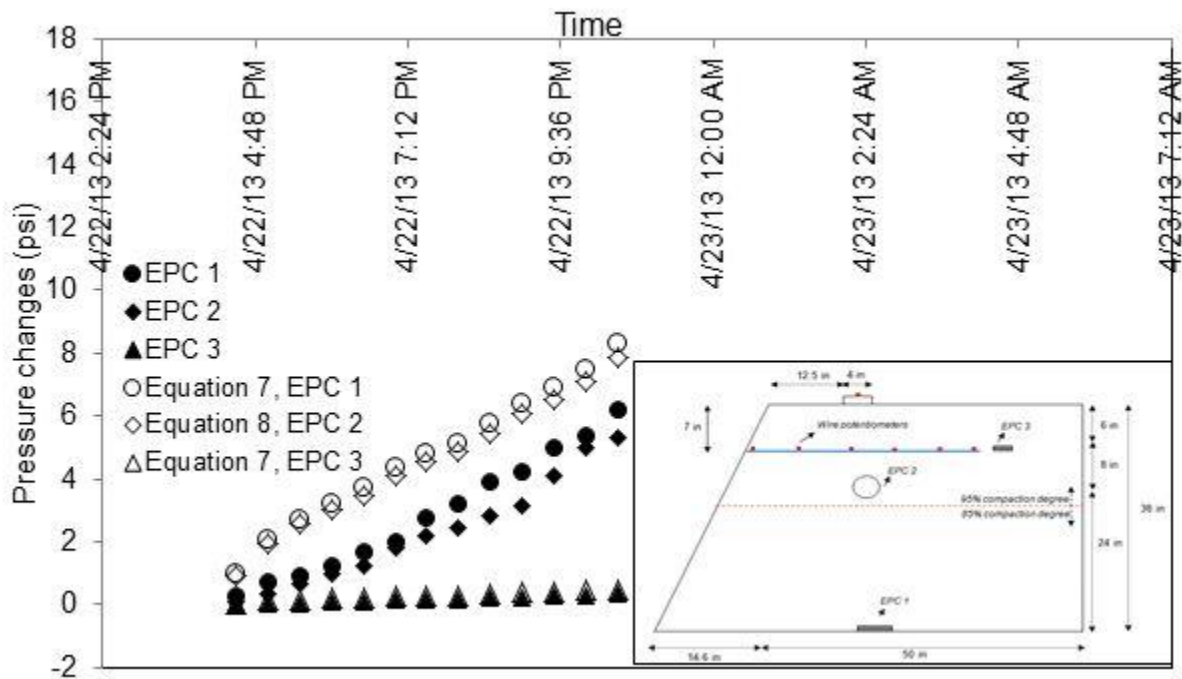
$$\Delta\sigma_y = \frac{2q\vartheta z}{\pi(x^2+z^2)} \quad (9)$$

Where:

- i.  $\Delta\sigma_y$ : Increase in horizontal stress
- ii.  $\vartheta$ : Soil Poisson's ratio



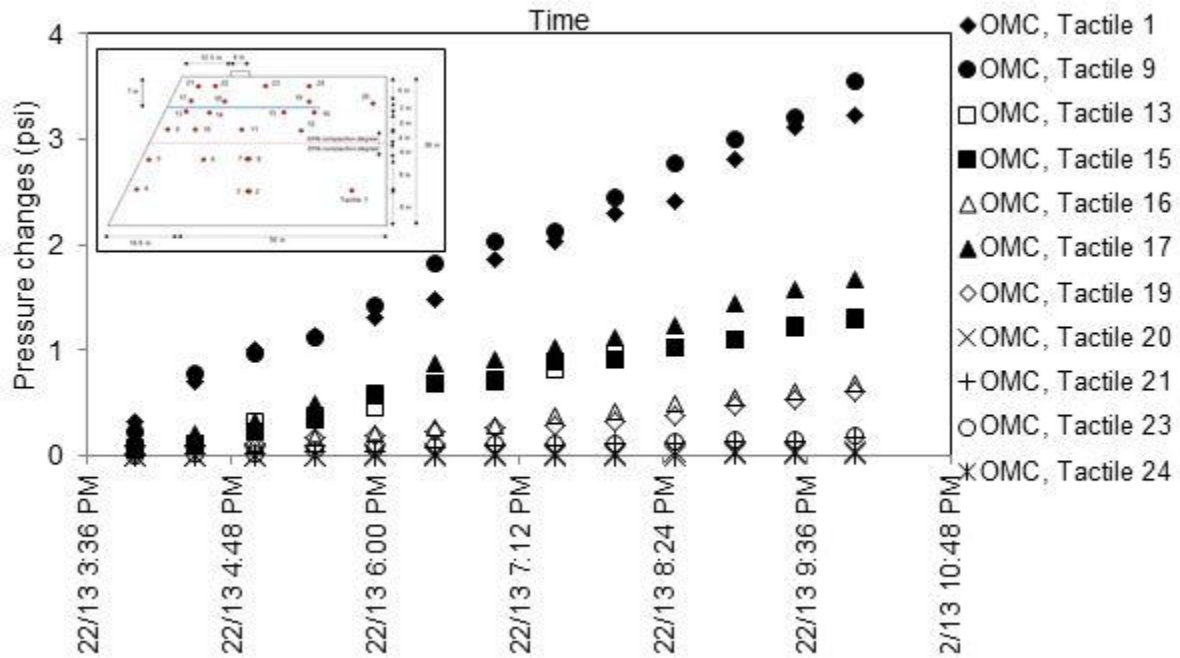
(a)



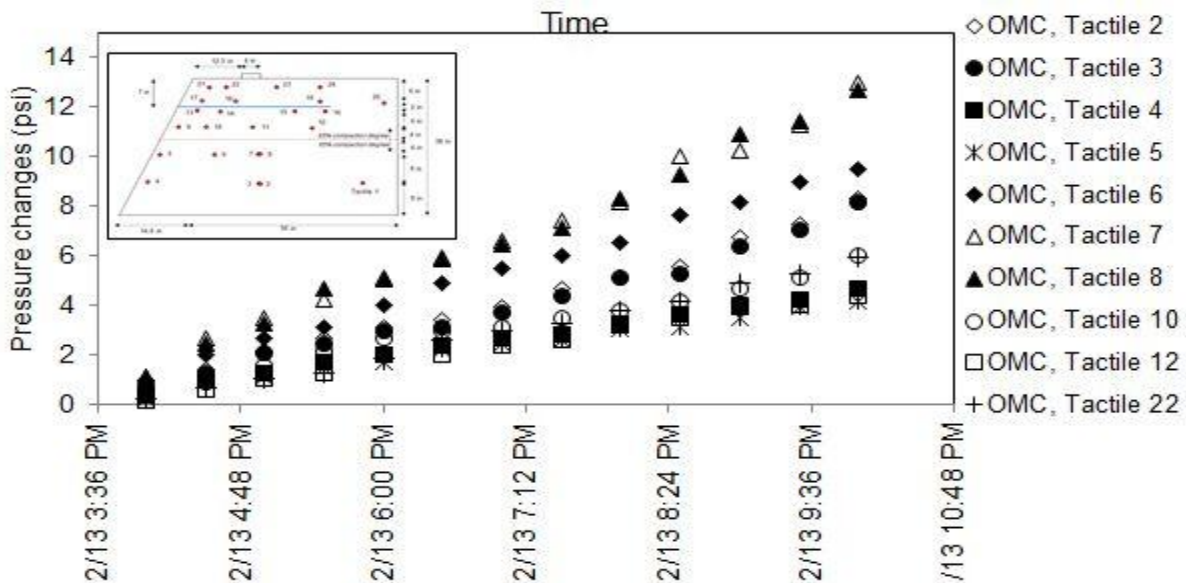
(b)

Figure 24. Comparison of the measured and theoretical predicted (Boussinesq method) incremental stresses due to the strip footing loading at selected locations in model embankments: (a) Test at OMC-2%, (b) Test at OMC

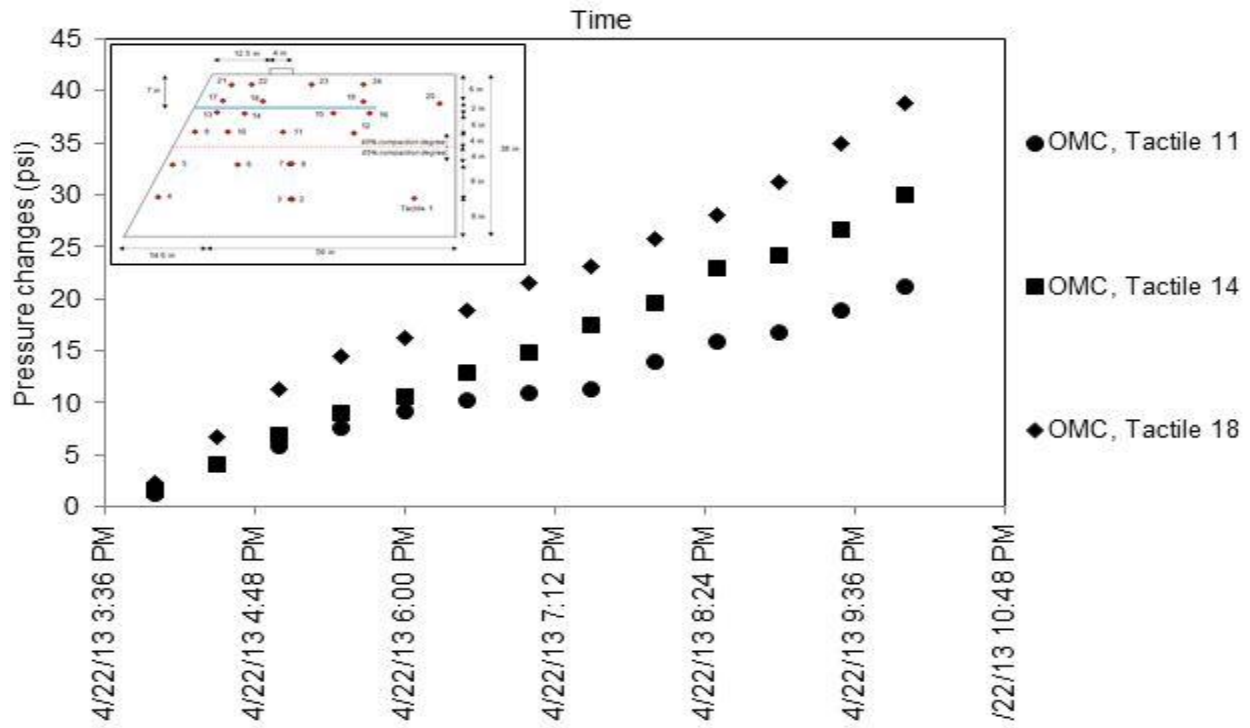
Results shown in Figure 24 indicate that the vertical pressures predicted from the Boussinesq equation are greater and more conservative than the measured values in all test cases shown. Figure 25 shows incremental vertical stresses inside the embankment during the loading stage until failure as recorded by the tactile sensors.



(a)



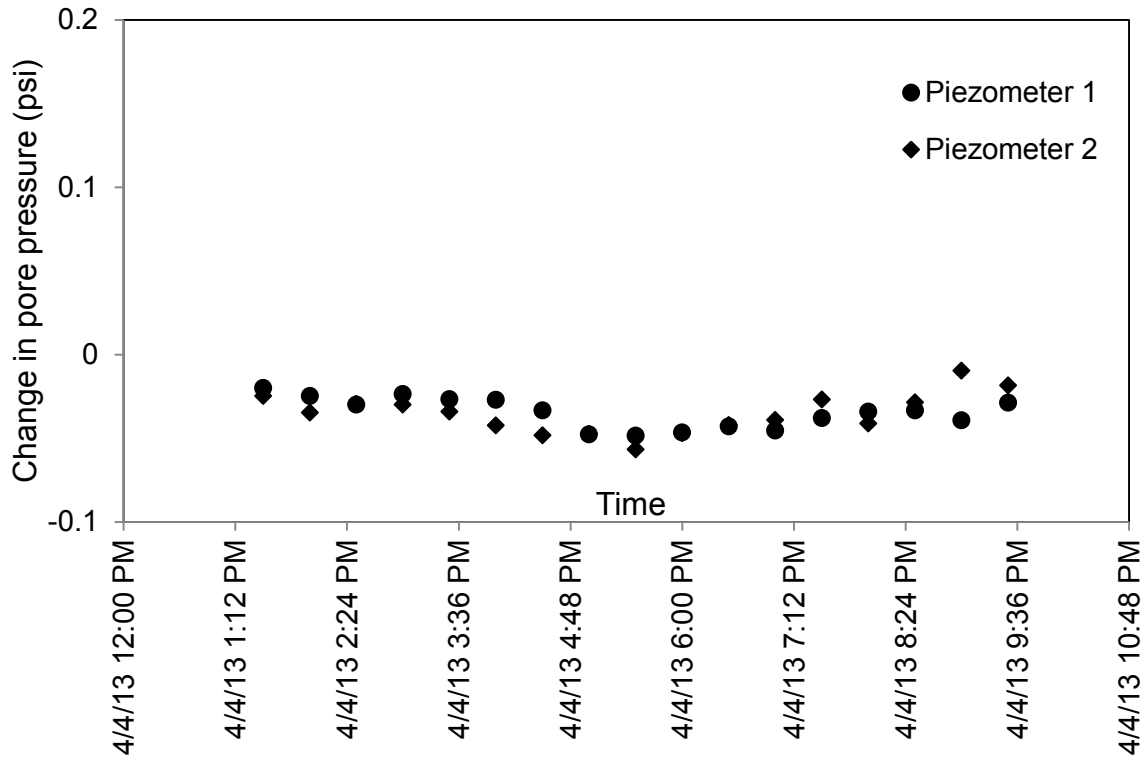
(b)



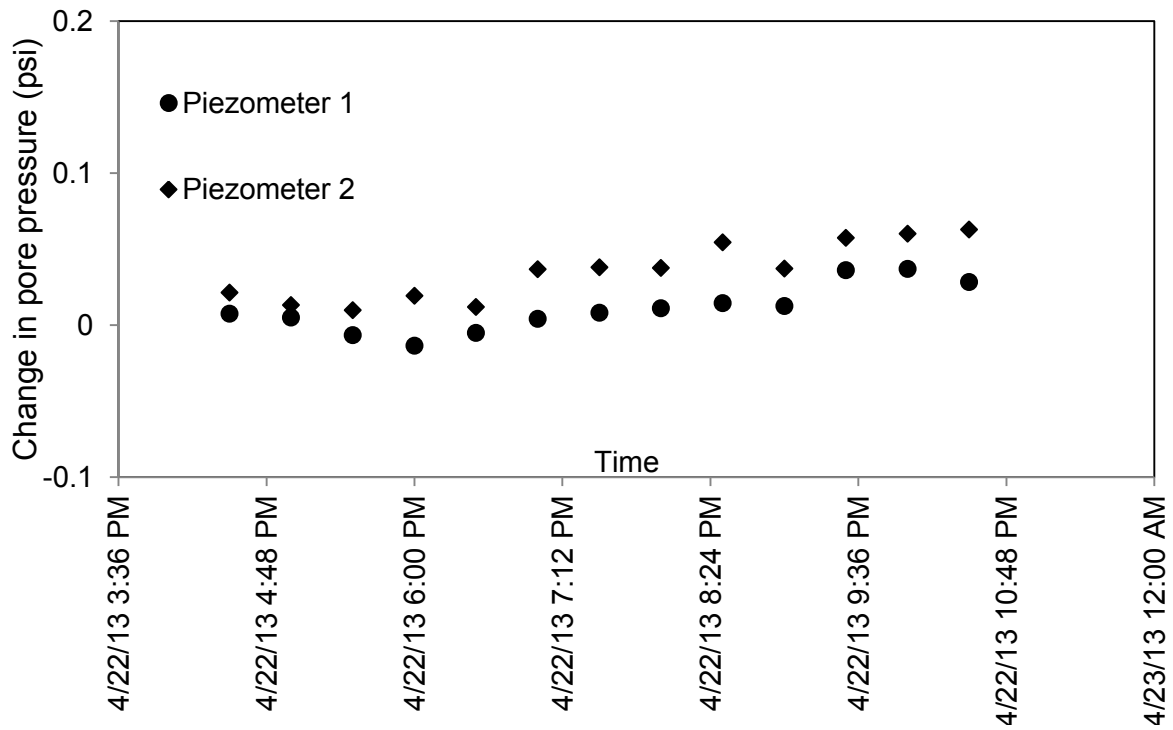
(c)

Figure 25. History of incremental earth pressures in the model embankment constructed at OMC subjected to footing loading

Figure 26 shows the pore pressure data measured by two piezometers in the embankment (Figure 8a, b). The results in Figure 25a indicate that no positive pore water pressure was developed in the drier model constructed at OMC-2% throughout the testing period. The data for the model embankment at OMC consistently show slightly greater positive pore pressure values. However, their magnitudes remain practically negligible throughout the testing period.



(a)



(b)

Figure 26. Changes in the pore water pressure as recorded by piezometers during surcharge loading: (a) Test at OMC-2%, (b) Test at OMC

### 6.2.6 Geotextile Strains

Geotextile strains and local displacements were measured using six (6) wire-line extensometers attached to different locations along the reinforcement length (Figures 8b and 27). Figure 28 shows the geotextile displacement versus vertical load on the embankment for the test at OMC-2%. The failure wedge in all three embankment models tested involved a bilinear slip plane that originated from the upstream side of the footing beam on the surface of the embankment and was intercepted by the reinforcement layer, forming a two-part wedge sliding block bracketed by the slip plane and the embankment facing (Figure 29). In Figure 29,  $L_{DS}$  and  $L_{IS}$  indicate the length of soil which sheared over the soil and geotextile reinforcement, respectively.

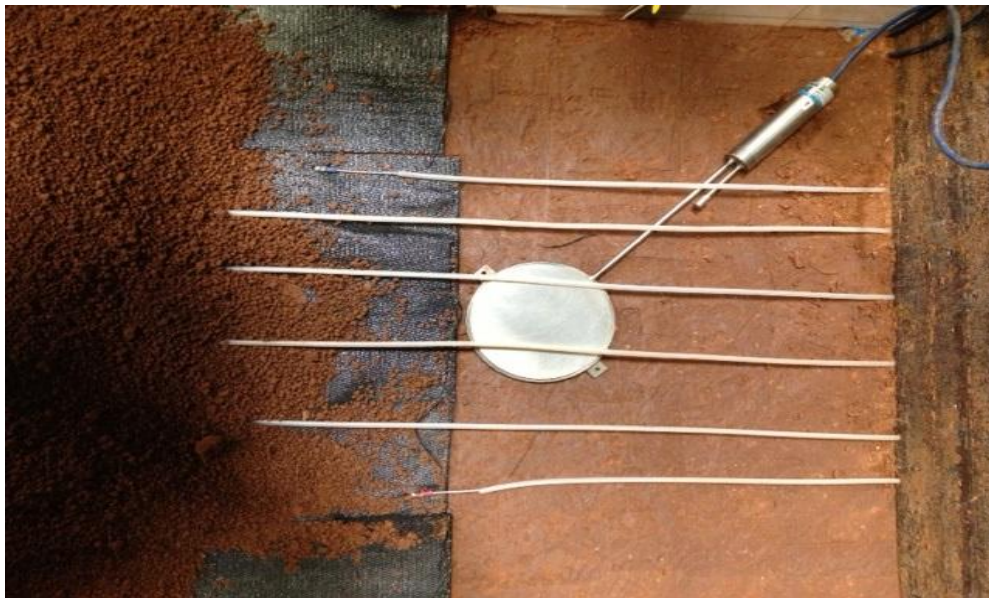
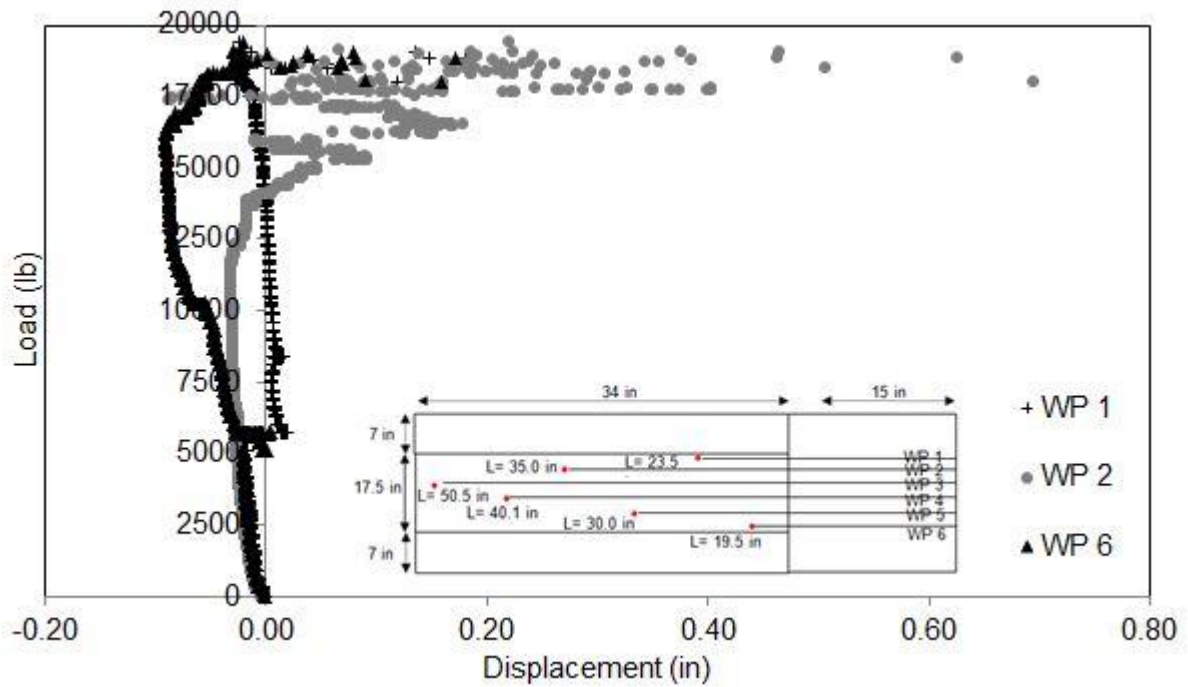
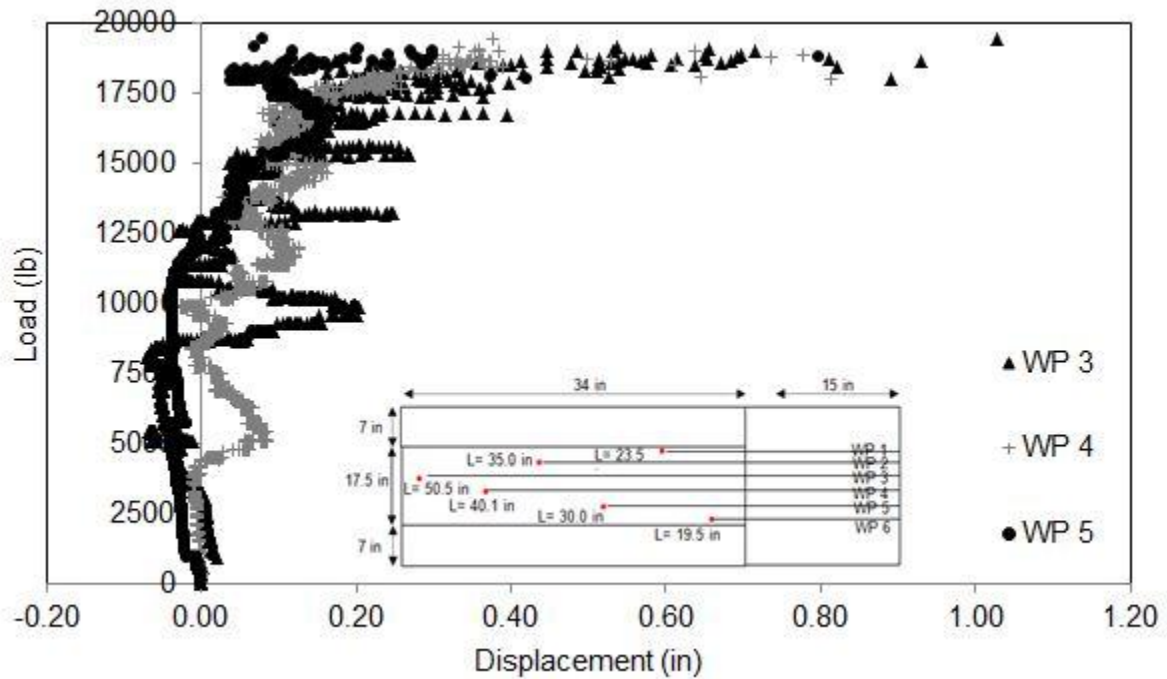


Figure 27. Wire-line extensometers attached to geotextile reinforcement to measure geotextile strains



(a)



(b)

Figure 28. Geotextile displacements as measured with attached wire potentiometers for the test at OMC-2%; (a) Displacement recorded by WPs 1, 2 and 6, (b) Displacement recorded by WPs 3, 4 and 5

Figure 29 shows the failure wedges formed at the end of the surcharge loading stage for the three test cases (i.e. OMC-2%, OMC and OMC+2%). After failure had occurred, the loading assembly was removed. Then, excavation started by carefully removing the soil of the failure wedges. The plexiglass sidewalls helped to trace the failure wedges so that the excavation process does not produce any additional cracks beyond the failure wedges. Figure 17b shows the embankment after the failure wedge had been excavated. The geometry of the failure wedges was measured, recorded and plotted in Figure 29. In all the test cases, the failure wedges formed at the back of the footing and propagated until they intercepted the geotextile reinforcement and continued along the soil-geotextile interface as opposed to penetrate through the geotextile. Since there was relatively negligible (i.e. almost zero) movement recorded by WP 6 (tail-end), the failures were defined as a combination of soil shearing and soil-geotextile interface shearing (i.e. without pullout of geotextile). These phenomena could be caused by the size of the embankment model (i.e. reduced-scale). Thus, the footing ultimate bearing capacity was not large enough to generate pullout failure.

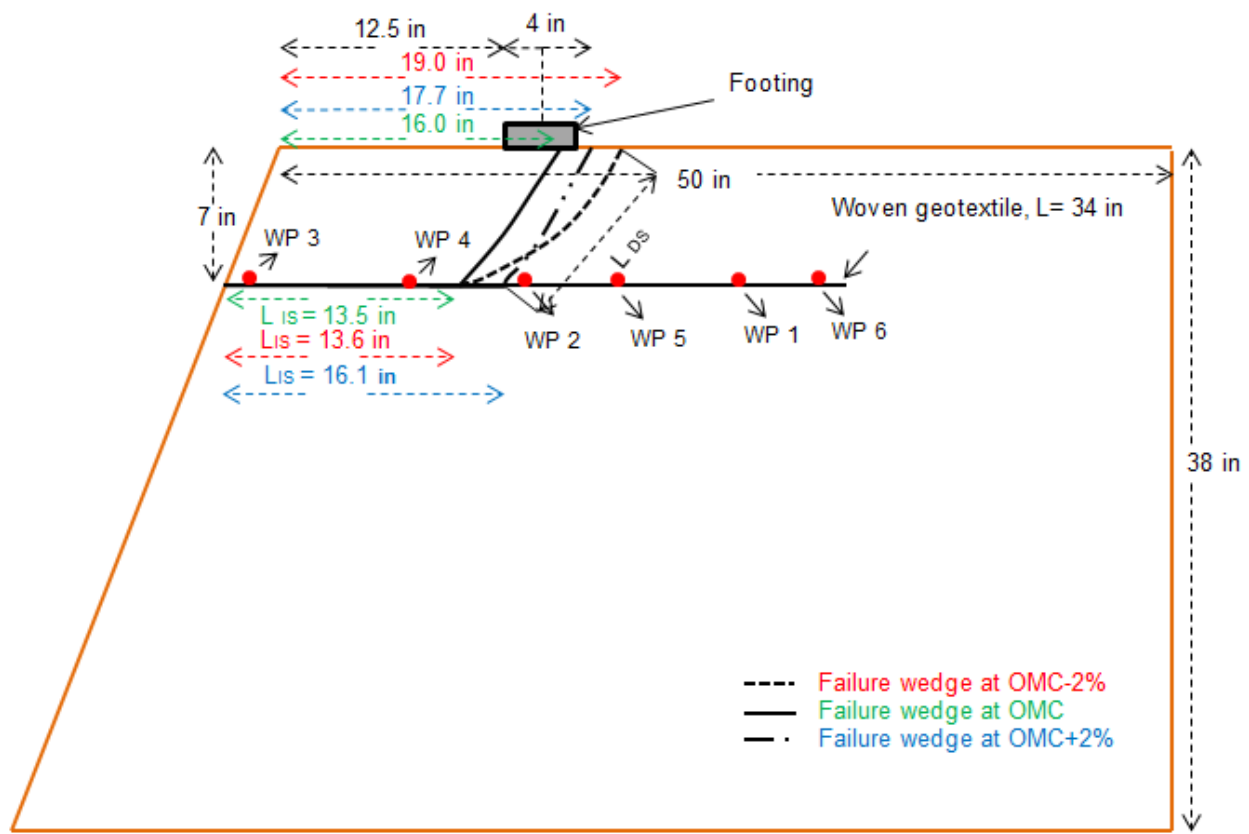


Figure 29. Diagram of the reinforced embankment and the failure wedges observed in test cases at OMC-2%, OMC, and OMC+2%

### 6.2.6.1 Strain Distributions

Figure 30 shows strain distributions over the length of the geotextile reinforcement at the failure vertical load on the strip footing. The value of local displacement at the point where failure wedge intercepted geotextile reinforcement was interpolated from displacements recorded by WP 2 and 4. Results in Figure 30 indicate that the strains in the geotextile reinforcement are greater at higher matric suction and lower gravimetric water content due to greater interface strength properties in a drier soil.

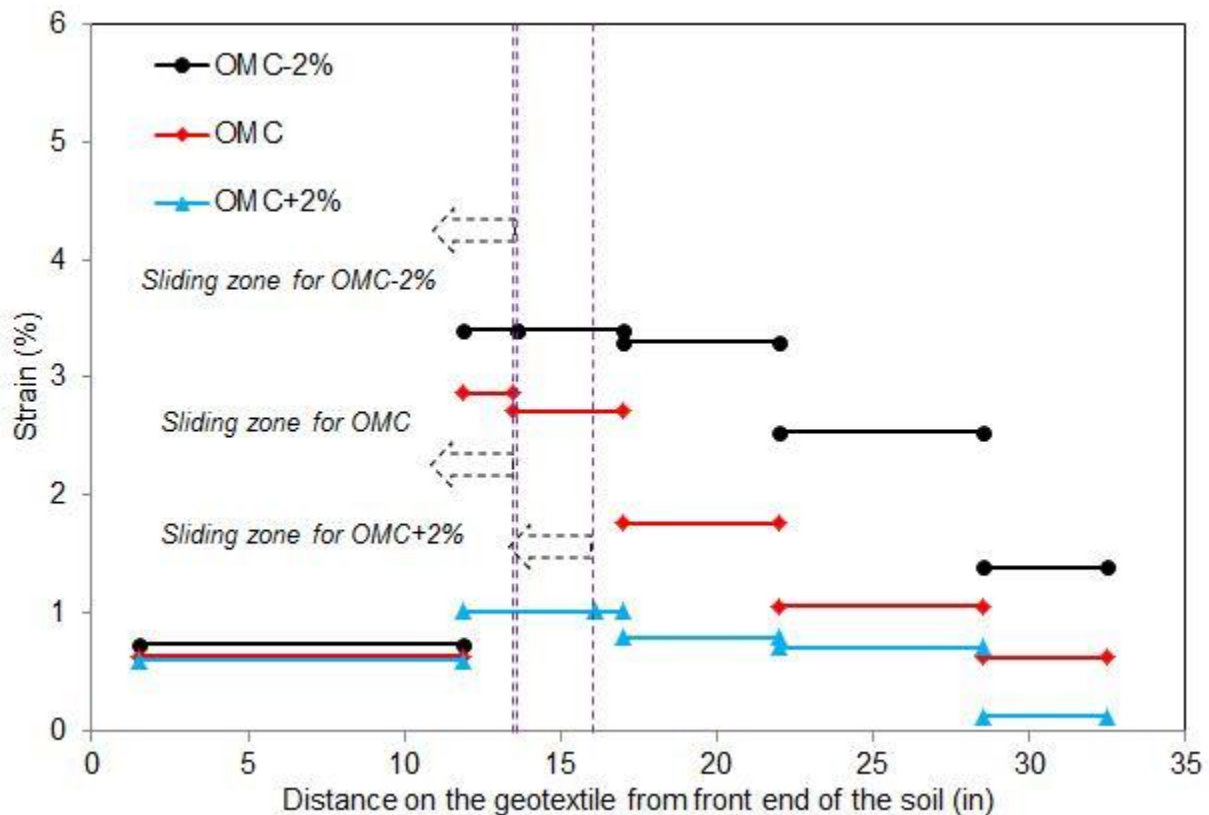
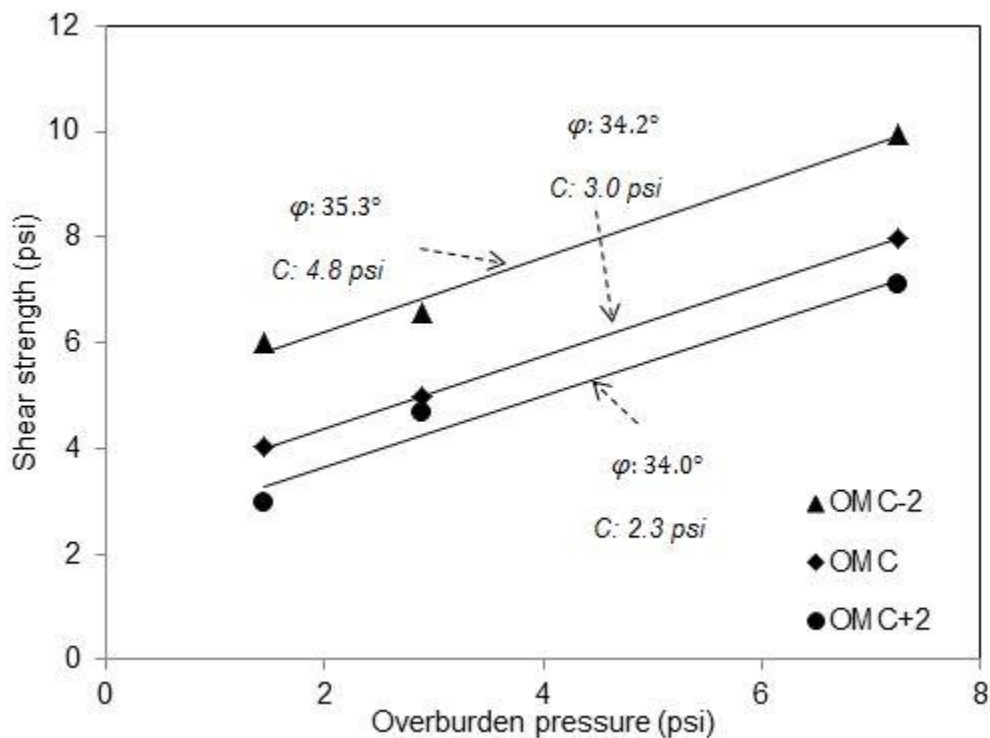


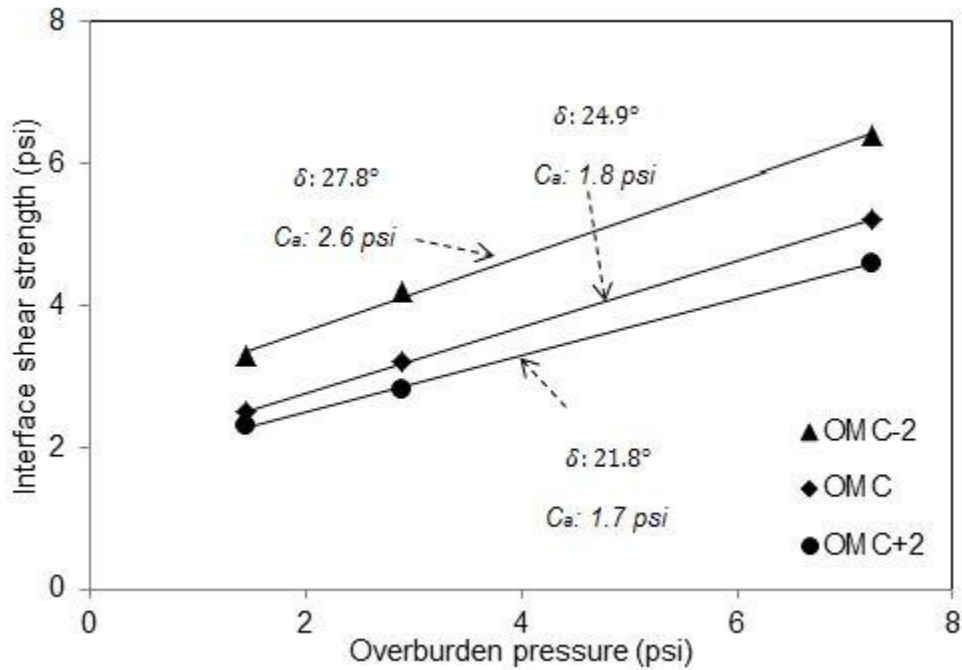
Figure 30. Strain distributions in the geotextile reinforcement in different model embankments at failure load

## 7. MOISTURE REDUCTION FACTOR, $\mu(\omega)$

Based on the results of this study, the observed failure wedges in all three test cases involved sliding a sheared block of soil over the geotextile reinforcement with comparatively insignificant pullout behavior. Therefore, it was concluded that Equation 2 would be primarily applicable to the soil-reinforcement performance as related to the stability of the soil mass in the model embankments tested which was modified in the form of Equation 4. As it is shown in Figure 29, shearing of embankment soil beneath the footing and its sliding over the reinforcement constitutes a likely failure mode in the stability analysis of reinforced soil embankments subjected to line loads such as those from bridge abutments. A series of small-scale (2.35 in  $\times$  2.35 in test cell) direct shear tests (DST) and interface shear tests (IST) were performed on the embankment soil and the woven geotextile to determine the shear strength properties of the soil and soil-the geotextile interface for the stability analysis of the model embankments. Figure 31 shows the DST and IST results.



(a)



(b)

Figure 31. (a) DST data on the embankment soil, (b) IST data on the embankment soil and woven geotextile

Figure 32 shows the  $\mu(\omega)$  values (i.e. MRF) for reduced-scale embankment tests calculated from Equation 9 as compared to the values obtained from the interface shear tests on the Chickasha soil and woven geotextile in a recent study by the authors (Hatami et al. 2011b).

$$\mu \omega \text{ for each test case} = \frac{c + \sigma'_v \tan \varphi_{L_{DS}} + c_a + \sigma'_v \tan \delta_{L_{IS}} \text{ for each test case}}{c + \sigma'_v \tan \varphi_{L_{DS}} + c_a + \sigma'_v \tan \delta_{L_{IS}} \text{ at OMC-2\%}} \quad (10)$$

Where  $L_{DS}$  and  $L_{IS}$  are defined in Figure 29 and  $c$ ,  $\varphi$ ,  $c_a$  and  $\delta$  are shear strength and interface shear strength parameters. The magnitude of  $\sigma'_v$  as applied to  $L_{DS}$  in Equation 9 was taken as the mean value of the normal stress over the length of the dipping slip plane above the geotextile reinforcement (i.e.  $L_{DS}$  in Figure 29) in the embankment soil in each test case.

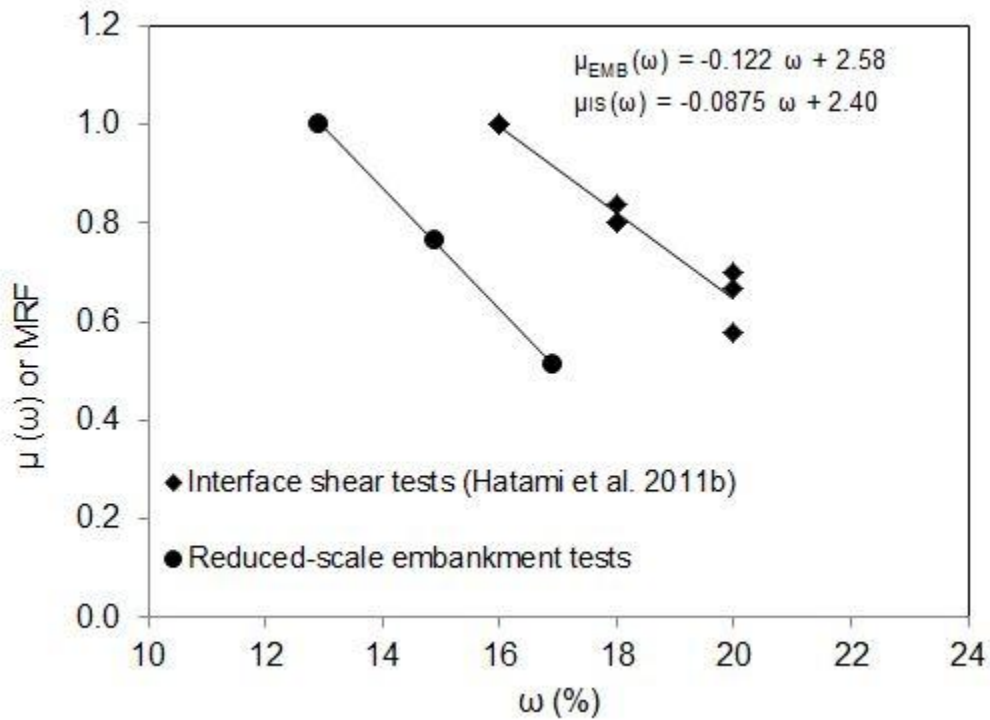


Figure 32. Moisture reduction factor,  $\mu(\omega)$ , for the woven geotextile in the embankment models in this study (i.e. from the borrow source CS 2780 in Chickasha, OK) as compared to the corresponding IST values for the soil from a nearby failed roadway embankment in a recent study by the authors (Hatami et al. 2011b)

Results shown in Figure 32 for the model embankment soil indicate that wetting of the soil and the soil-geotextile interface during construction or service life of reinforced soil slopes could significantly reduce their shear strength resulting in lower factors of safety against their instability. From the data shown in Figure 32, the moisture reduction factors (i.e.  $\mu(\omega)$  or MRF) for the model embankments and the IST for a change in the soil GWC value from OMC-2% to OMC+2% are approximately 50% and 60%, respectively. These values indicate that the reduction in the soil-reinforcement shear strength in the embankment models is comparable to that observed from the IST data. Therefore, the IST MRF values appear to provide reasonable estimates of the design values for model embankments. However, additional tests on a wider range of soils and reinforcing materials are needed to verify or modify this conclusion.

## 8. CONCLUSIONS

The primary objective of this study was to develop a moisture reduction factor [MRF or  $\mu(\omega)$ ] for the shear strength of soil-geotextile reinforcement interface for the stability analysis and design of reinforced soil structures constructed with marginal soils. The  $\mu(\omega)$  values were determined through a series of reduced-scale embankment tests in the laboratory.

Results from the embankment tests in this study indicated that the change in the soil matric suction and gravimetric water content (GWC) could have a significant influence on the soil-geotextile reinforcement interface strength. The results of the study showed that within the range of GWC values examined (i.e. OMC  $\pm$  2%), the embankment model constructed at OMC-2% yielded the greatest shear strength and stability when subjected to a line surcharge load simulating loading from bridge abutments. The MRF values from the embankment tests were found to be comparable with those from interface shear tests (IST) in the authors' earlier study. However, correction factors might have to be applied on laboratory test data to account for the embankment geometry and soil type (among other possible factors) in the calculation of the MRF values for the design of field embankments.

## 9. REFERENCES

- Adams, M. T. and Collin, J. G., 1997, "Large Model Spread Footing Load Tests on Geosynthetic Reinforced Soil Foundations," *Journal of Geotechnical and Geoenvironmental Engineering, ASCE, Vol. 123, No. 1, pp. 66- 72.*
- American Association of State Highway and Transportation Officials, AASHTO, 2008, "Guide Specifications for Design and Construction of Segmental Concrete Bridges," Second Edition, Washington, DC, <http://www.transportation.org/>
- ASTM International, 2006, "Standard Test Method for Amount of Material in Soils finer than No. 200 (75- $\mu$ m) Sieve," *American Society for Testing and Materials, West Conshohochen, PA, USA.*
- ASTM International, 2007, "Standard Test Method for Particle Size Analysis of Soils," *American Society for Testing and Materials, West Conshohochen, PA, USA.*
- ASTM International, 2009, "Standard Test Method for Tensile Properties of Geotextiles by the Wide-Width Strip Method," *American Society for Testing and Materials, West Conshohochen, PA, USA.*
- ASTM International, 2010, "Standard Test Method for Laboratory Determination of Water (Moisture) Content of Soil and Rock by Mass," *American Society for Testing and Materials, West Conshohochen, PA, USA.*
- Bathurst, R. J., Blatz, J. A. and Burger, M. H., 2003, "Performance of Instrumented Large-Scale Unreinforced and Reinforced Embankments Loaded by a Strip Footing to Failure," *Canadian Geotechnical Journal, Vol. 40, No. 6, pp. 1067-1083.*
- Berg R.B., Christopher, B.R. and Naresh C. Samtani, 2009, "Design and Construction of Mechanically Stabilized Earth Walls and Reinforced Soil Slopes," *Federal Highway Administration, Washington, DC, USA, FHWA-NHI-10-024.*
- Budhu, M., 2000, "Soil Mechanics and Foundations," *John Wiley & Sons, Inc.*
- Campbell, G.S. and W.H. Gardner.1971, "Psychometric Measurement of Soil Water Potential: Temperature and Bulk Density Effects," *Soil Science Society of America Proceedings, Vol.35. pp. 8-11.*
- Elias, V., Christopher, B.R. and Berg, R.R., 2001, "Mechanically Stabilized Earth Walls and Reinforced Soil Slopes-Design and Construction Guidelines," *Federal Highway Administration, Washington, DC, USA, FHWA-NHI-00-043.*
- Fredlund, D.G., Morgenstern, N.R., and Widger, R.A., 1978, "The Shear Strength of Unsaturated Soils," *Canadian Geotechnical Journal, Vol. 15, No. 3, pp. 313-321.*
- Geokon, Inc., 2013, "Earth Pressure Cells, 3500, 4800 Series," *Geokon, Inc., Lebanon, NH, USA, [http://www.geokon.com/content/datasheets/4800\\_Series\\_Earth\\_Pressure\\_Cells.pdf](http://www.geokon.com/content/datasheets/4800_Series_Earth_Pressure_Cells.pdf)*
- Georgiadis, K., 2010, "Undrained Bearing Capacity of Strip Footings on Slopes," *Journal of Geotechnical and Geoenvironmental Engineering, ASCE, Vol. 136, No. 5, pp. 677-685.*
- Germer, K., Farber, A. and Braun, J., 2008, "Studies on Slope Failure Process in a Laboratory Flume," *Geophysical Research Abstracts, Vol. 10, EGU2008-A-05633, pp. 115-118.*

- Hatami, K., Miller G.A., and Garcia L., 2010a, "Use of MSE Technology to Stabilize Highway Embankments and Slopes in Oklahoma," *Oklahoma Department of Transportation, Tulsa, OK, USA, Final Report OTC REOS7-1-19*.
- Hatami K., Garcia L.M. and Miller, G.A., 2010b, "Influence of moisture content on the pullout capacity of geotextile reinforcement in marginal soils," *61<sup>st</sup> Highway Geology Symposium, Oklahoma City, OK*.
- Hatami K., Garcia L.M. and Miller G.A., 2011a, "A Moisture Reduction Factor for Pullout Resistance of Geotextile Reinforcement in Marginal Soils," *Geo-Frontiers, Dallas, TX, ASCE Special Publication No. 211*.
- Hatami, K., Miller G.A., and Esmaili D., 2011b, "Use of MSE Technology to Stabilize Highway Embankments and Slopes in Oklahoma," *Oklahoma Department of Transportation, Oklahoma City, OK, USA, Final Report FHWA-11-04, ODOT SPR Item 2214*.
- Huang, C. C., Tatsuoka, F. and Sato, Y., 1994, "Failure Mechanism of Reinforced Sand Slopes Loaded with a Footing," *Soils and Foundations Journal, Vol. 34, No. 2, pp. 27-40*.
- Itasca Consulting Group Inc, 2005, *Fast Lagrangian Analysis of Continua: FLAC, Version 5.0*, Minneapolis, MN, 2011.
- Keller, G.R., 1995, "Experiences with Mechanically Stabilized Structures and Native Soil Backfill," *Transportation Research Record, 1474: 30-38*.
- Kumar, A., Ohri, M. L. and, Bansal, R. K., 2007, "Bearing Capacity Tests of Strip Footings on Reinforced Layered Soil," *Geotechnical and Geological Engineering Journal, Springer, Vol. 25, No. 2, pp. 139-150*.
- Kumar, A. and Saran, S., 2003, "Closely Spaced Footings on Geogrid-Reinforced Sand," *Journal of Geotechnical and Geoenvironmental Engineering, ASCE, Vol. 129, No. 7, pp. 660-664*.
- Lee, K. M. and Manjunath, V. R., 2000, "Experimental and Numerical Studies of Geosynthetic Reinforced Sand Slopes Loaded with a Footing," *Canadian Geotechnical Journal, Vol. 37, No. 4, pp. 828- 842*.
- Lee, K. M. and Manjunath, V. R. and Dewaikar, D. M., 1999, "Numerical and Model Studies of Strip Footing Supported by a Reinforced Granular Fill-Soft Soil System," *Canadian Geotechnical Journal, Vol. 36, No. 5, pp. 793- 806*.
- Miller, G.A. and Hamid, T.B., 2005, "Direct Shear Testing of Interfaces in Unsaturated Soil," *Proceedings of EXPERUS, International Symposium on Advances in Experimental Unsaturated Soil Mechanics, Trento, Italy*.
- Myers, B.K. and Scofield, D.H., 2006, "Providing Improved Dam Safety Monitoring Using Existing Staff Resources: Fern Ridge Dam Case Study,"  
[http://www.engineeredmonitoringsolutions.com/Automated Dam Safety Monitoring Fern Ridge Dam.pdf](http://www.engineeredmonitoringsolutions.com/Automated_Dam_Safety_Monitoring_Fer_n_Ridge_Dam.pdf)
- Ou, F.L., Cox, W. and Collett, L., 1982, "Rock Aggregate Management Planning for Energy Conversation: Optimization methodology," *Transportation Research Record, 872: 63-69*.
- Sako, K., Kitamura, R. and Fukagawa, R., 2006, "Study of Slope Failure Due to Rainfall: a Comparison between Experiment and Simulation," *Proceedings of 4<sup>th</sup> International Conference on Unsaturated Soils, ASCE, Carefree, USA, Vol. 2, pp. 2324-2335*.

- Sawwaf, M. E. and Nazir, A., 2012, "Behavior of Eccentrically Loaded Small-Scale Ring Footings Resting on Reinforced Layered Soil," *Journal of Geotechnical and Geoenvironmental Engineering, ASCE, Vol. 138, No. 3, pp. 376-384.*
- Sensor Products Inc., 2013, <http://www.sensorprod.com/tactilus.php>
- Sitharam, T. G., Sireesh, S. and Kumar Dash, S., 2005, "Model Studies of a Circular Footing Supported on Geocell-Reinforced Clay," *Canadian Geotechnical Journal, Vol. 42, No. 2, pp. 693-703.*
- Thanapalasingam, J. and Gnanendran, C. T., 2008, "Predicting the Performance of Foundations Near Reinforced Sloped Fills," *the 12<sup>th</sup> International Conference of International Association for Computer Methods and Advances in Geomechanics, India, pp. 3727-3734.*
- Tohari, A., Nishigaki, M. and Komatsu, M., 2007, "Laboratory Rainfall-Induced Slope Failure with Moisture Content Measurement," *Journal of Geotechnical and Geoenvironmental Engineering, ASCE, Vol. 133, No. 5, pp. 575-587.*
- Wescor Inc., 2001, HR-33T Dew Point Microvoltmeter Instruction/Service Manual. *Wescor Inc., Lohan, UT, <http://water.wescor.com/hr33t.html>.*